



Role of biopolymers as major carrier phases of Th, Pa, Pb, Po, and Be radionuclides in settling particles from the Atlantic Ocean

Chia-Ying Chuang^{a,*}, Peter H. Santschi^a, Yi-Fang Ho^a, Maureen H. Conte^b, Laodong Guo^c, Dorothea Schumann^d, Marin Ayrarov^e, Yuan-Hui Li^f

^a Department of Marine Sciences and Oceanography, Texas A&M University, Galveston, TX 77553, USA

^b Bermuda Institute of Ocean Sciences, Bermuda and Ecosystems Center, MBL, Woods Hole, MA 02543, USA

^c School of Freshwater Sciences, University of Wisconsin-Milwaukee, Milwaukee, WI 53204, USA

^d Paul Scherrer Institute, CH-5232 Villigen, Switzerland

^e European Commission, DG-Energy, Luxembourg

^f Department of Oceanography, University of Hawaii at Manoa, 1000 Pope Road, Honolulu, HI 96822, USA

ARTICLE INFO

Article history:

Received 13 May 2013

Received in revised form 26 September 2013

Accepted 2 October 2013

Available online 9 October 2013

Keywords:

Particle reactive radionuclides

Sediment trap particles

Oceanic Flux Program

Particle flux

Hydroxamate siderophores

Calcite

Biogenic silica

Iron

Manganese

Thorium

Protactinium

Lead

Polonium

Beryllium

ABSTRACT

The concentrations of potential organic (e.g., proteins, polysaccharides, uronic acids, hydroquinones, hydroxamate- and catechol-type siderophores) and inorganic (Fe, Mn, Si, and CaCO₃) carrier phases for radionuclides (²³⁴Th, ²³³Pa, ²¹⁰Po, ²¹⁰Pb and ⁷Be) and their particle–water partition coefficients (*K_d*) were determined for particles collected by sediment traps deployed at the Oceanic Flux Program (OFF) site off Bermuda (500, 1500 and 3200 m). The purpose was to better understand the mechanisms that control the chemical composition of sinking particles as well as the scavenging and fractionation behavior of those five radionuclides. Different components contributed differently to the scavenging of different radionuclides at the three depths. Chemical considerations (e.g., ionic potential, ionization energy, multifunctional group structures), as well as factor analysis (FA) and correlations of log*K_d* values with chemical parameters, indicate that hydroxamate siderophores are major classes of biopolymers that have a role in binding Po and Pa. MnO₂ and FeO₂, whose presence is closely related to that of hydroxamate siderophores (HS), are also involved in binding of Pa and Po. The carbonate and biogenic silica phases are identified to be important in predicting removal and fractionation of Th and Be in the ocean.

© 2013 Elsevier B.V. All rights reserved.

1. Introduction

Natural particle-reactive radionuclides, such as ^{230,234}Th, ²³¹Pa, ²¹⁰Po, ²¹⁰Pb and ^{7,10}Be, have been widely used for decades as important proxies to understand oceanic processes, such as boundary scavenging, particle flux, paleo-circulation and water mass residence times (Broecker and Peng, 1982). However, the interactions and binding relationships between radionuclides and components of marine particles as well as the molecular level bonding mechanisms remain poorly understood (Santschi et al., 2006). Though radioisotopic tracers can be applied without knowledge of specific mechanisms, the lack of a fundamental understanding of radionuclide scavenging and partitioning

can fuel heated scientific controversies over the interpretations of tracer data (e.g., Li, 2005).

Generally, speciation and transport of the low concentrations of natural radionuclides (at ~pico- to femto- or attomolar concentrations) in the ocean are governed by thermodynamic and kinetic processes in adsorptive uptake and transport by organic or inorganic particles. Given that the concentrations of the ions of natural radionuclides are in the sub-picomolar range, while concentrations of organic and inorganic colloids and particles in surface waters are in the micromolar range (Santschi et al., 1995, 2002), most radionuclide ions are unlikely to form their own hydrolytic species but tend to associate with a carrier phase by binding to certain functional groups in colloidal and particulate surfaces. There is considerable evidence to support this contention, for example, the associated particles containing hydrolyzed aluminosilicates and Fe–Mn oxides (Doucet et al., 2001; M.A. Kim et al., 2003; Panak et al., 2003), Fe-organic colloids (Santschi et al., 2002), and

* Corresponding author at: 200 Seawolf Parkway, Texas A&M University at Galveston, Galveston, TX, 77553, USA. Tel.: +1 409 740 4530; fax: +1 409 740 4786.

E-mail address: anderin@tamu.edu (C.-Y. Chuang).

polysaccharide-rich exopolymeric substances (Guo et al., 2002a,b; Quigley et al., 2002; Roberts et al., 2009; Xu et al., 2009, 2011).

Most natural radionuclides have metal characteristics and are subject to chelation by organic ligands such as siderophores that are the major class of metal chelators in the aquatic environment. Siderophores, a group of high-affinity metal-binding ligand compounds, are secreted by microorganisms in response to the need for soluble Fe, which is present at very low concentrations in oceanic waters (Reid et al., 1993; Neilands, 1995; Winkelmann, 2002). The structural features and chemical composition of siderophores are diverse. The functional groups contain oxygen atoms of hydroxamate, catecholate, α -hydroxy carboxylic and salicylic acids, or nitrogen atoms of oxazoline and thiazoline. In seawater, it has been well documented that 99% or more of water-soluble Fe, especially the ferric ion, Fe(III), is bound to dissolved organic ligands, including siderophores (Gledhill and Van Den Berg, 1994; Rue and Bruland, 1995; Boye et al., 2001; Mawji et al., 2008; Kondo et al., 2012). In the particle phase, however, the existence of siderophores has, so far, not been documented. Additionally, siderophores could also complex metals other than Fe(III), including natural radionuclides such as Pu(IV) and Th(IV) (Neu et al., 2000; Keith-Roach et al., 2005), which have similar physicochemical properties as the ferric iron.

To evaluate potential carrier phases controlling the speciation and scavenging of particle-reactive radionuclides in the ocean, we have comprehensively examined the composition of sinking particles collected by the Oceanic Flux Program (OFP) sediment traps deployed in the northern Sargasso Sea off Bermuda. The abundance of potential organic carriers, including proteins, total polysaccharides, uronic acids, hydroquinones, and hydroxamate-type and catechol-type siderophores, as well as inorganic phases (Mn, Fe, Si, and CaCO_3) in the particles was quantified. The purpose was to examine their possible correlation with the particle–water partitioning coefficients of ^{234}Th , ^{233}Pa , ^{210}Po , ^{210}Pb and ^7Be . To the best of our knowledge, this is the first time that the functionalities of hydroxamate siderophores (HS) in marine particles are studied and implicated to be important for radionuclide binding. The chemical relationships and statistical analyses reported here provide new insights into the relative importance of organic and inorganic carrier phases for different radionuclides with clear evidence that HS is involved in a major way in the binding and removal of specific radionuclides in marine particles.

2. Methods

2.1. Sediment trap sampling

The Bermuda Oceanic Flux Program (OFP) time-series site is located at 31° 50' N, 64° 10' W with water depth of 4500 m. Sediment trap mooring system, sample processing and analytical protocols have been previously described (Conte et al., 2001; Huang and Conte, 2009). McLane Parflux sediment traps (0.5 m² surface area; McLane Labs, Falmouth, MA, USA) are positioned at 500, 1500 and 3200 m depths and programmed at about 2-week sampling resolution. Sample cups are filled with high purity seawater brine (salinity of 40) that is prepared by freezing Sargasso Sea deep water (3000 m depth). The trap cup brine is preserved using ultra-high purity HgCl_2 (200 mg/l) to arrest biological degradation during sample collection.

2.2. Chemical analysis of sediment trap samples

Sediment trap samples were analyzed for dry weight, carbonate and organic carbon/nitrogen contents using methods detailed in Conte et al. (2001) and Huang and Conte (2009). Carbonate was determined by coulometry (Coulometrics). Organic carbon and nitrogen concentrations and isotopic composition were measured on a mass spectrometer (Europa 20–20 CF-IRMS interfaced with the Europa ANCA-SL elemental analyzer), after acidification of the samples by sulfurous acid to remove

carbonates. Elemental composition was determined using a small sample LiBO_2 fusion/ICPMS method (Huang et al., 2007).

Subsamples of archived OFP sediment trap materials (<125 μm size fraction) were transferred to the Texas A&M University at Galveston for additional analyses for select organic and inorganic phases, and for the determination of partition coefficients of radionuclides between particle and water phases in laboratory. Sixty one samples collected between the years 2004 to 2006 were analyzed: 14 samples from 500 m depth, 22 samples from 1500 m depth and 25 samples from 3200 m depth.

Mn and Fe contents in subsamples (<125 μm) were measured by an atomic absorption spectrometer (Varian) after overnight digestion with 12 N HNO_3 at 85 °C. Silica content of OFP sample was analyzed, after digestion, by a colorimetric method adopted from Strickland and Parsons (1972). The digestion method was modified from Hauptkorn et al. (2001). In brief, a mixture of 250 μl of Milli-Q and a 200 μl of 25% TMAH was added to ~1 mg OFP subsample followed by 30 min sonication. The solution was heated to 95 °C for overnight. The silicate concentration was determined in the supernatant fraction after centrifuging the solution at 3200g for 10 min. Additional data on the elemental concentrations in the OFP samples has been reported in Huang and Conte (2009).

Total carbohydrate concentrations of OFP subsamples (TCHO) were determined by the TPTZ (2,4,6-tripyridyl-s-triazine, Sigma) method using glucose as the standard (Hung and Santschi, 2001). Proteins were analyzed by a modified Lowry protein assay, using bovine serum albumin (BSA) as the standard (Pierce, Thermo Scientific). Uronic acids (URA) were determined by the meta-hydroxyphenyl method, using glucuronic acid as the standard (Filisetti-Cozzi and Carpita, 1991; and modified by Hung and Santschi, 2001). Hydroquinone (HQ) determination was modified from Sirajuddin et al. (2007), using hydroquinone as the standard. Thirty samples were selected to measure particulate hydroquinone. In brief, a 300 μl of Milli-Q water was added to ~1 mg particulate sample, and the solution was sonicated for an hour. The solution was then centrifuged (3500g, 5 min) to separate the particles from the supernatant. A 300 μl aliquot of 100 μM KMnO_4 was added to 100 μl of the particle–water mixture and reacted for 15 min under room temperature. The hydroquinone concentration was then determined by UV–Vis spectrophotometry at 288 nm.

Hydroxamate siderophore (HS) concentrations were measured by the Csaky's (1948) method, using acetohydroxamic acid (AHA) as the standard. Catechol siderophores were analyzed by Arnow's method, using catechol as the standard (Arnow, 1937). However, no catechol siderophores were detected in all OFP samples. Separate measurements of hydroxamate siderophores were carried out on three different sample fractions, namely, the water/methanol extract, the supernatant after 6N HCl digestion (110 °C, 24 h), and refractory particulate material remaining after acid digestion. Results showed that HS was only detectable in the acid digestible fraction, indicating that HS moieties are strongly bound to materials that are solubilized only under more extremely acidic conditions.

To assess potential artifacts and interferences in the colorimetric methods (e.g., potential interference of HS on TPTZ analysis; effects of polysaccharides concentration on HS determination), many in-depth cross-calibration experiments were also conducted. A serial AHA standards with different concentrations was applied for the TPTZ method to examine whether there is any absorbance at the characteristic wavelength for polysaccharides. These experiments did identify AHA interference in the spectrophotometric determination of TCHO. An appropriate correction was therefore applied to the raw TCHO concentrations data to eliminate the effects of AHA. No other interferences or artifacts were found.

2.3. Sorption experiments

Natural seawater (salinity of 35) collected from the Gulf of Mexico with background low molecular weight DOC was used for all sorption

experiments. The seawater was prepared by sequentially filtering seawater through a 0.2 μm polycarbonate cartridge, followed by filtering through a 1 kDa ultrafiltration membrane to remove particulate and colloidal organic matter (Guo et al., 1995; Roberts et al., 2009).

The ^{234}Th tracer was purified and extracted from a ^{238}U stock solution (Quigley et al., 2002; Alvarado Quiroz et al., 2006). ^{233}Pa , in equilibrium with ^{237}Np , was obtained from Pacific Northwest National Laboratory was used. ^{210}Pb and ^{210}Po , in 2 N HCl, were purchased from Eckert & Ziegler Isotope Products. The ^7Be tracer solution (in 0.5 N HCl) was manufactured at the Paul Scherrer Institute, Switzerland (Schumann et al., 2013).

^{233}Pa was added in equilibrium with ^{237}Np , whose activities could be found only in the dissolved phase for all samples, supporting the assumption that ^{237}Np would not adsorb onto particles during the experiment, thus justifying the decay and in-growth corrections of ^{233}Pa in solution only.

The design of the sorption experiment was modified from that of Roberts et al. (2009). Specifically, a non-complexing 20 mM/10 mM Tris–HCl buffer was transferred into acid cleaned experimental tubes to precondition the container walls for at least 24 h to reduce tracer adsorption. The reason for using Tris–HCl is that its buffer capacity also can neutralize the acidic radionuclide tracer solutions to avoid pseudo-colloids generation by normally used NaOH, and maintains the pH at 8.0 ± 0.5 . A small drop in pH was only occurring right at the beginning after the addition of the acidic tracer solution due to a limited buffer capacity, but the pH stayed constant throughout the experiment.

Each experiment was performed in duplicate. Ten milliliters of seawater was added to the preconditioned tube, and then between 10 and 15 Bq of radionuclide tracers (at equilibrium) was added. Solutions were then gently shaken and left to equilibrate overnight. The next morning trap particles were added to the seawater, resulting in a final particulate concentration of 10 mg/l. This concentration is within the range of suspended particulate matter concentrations in natural seawaters (National Research Council, 1972), which ranges from <1 mg/l in open ocean waters (Guo et al., 1997), to tens to >100 mg/l in the near-shore marine environment and estuarine waters (e.g., Baskaran and Santschi, 1993; Woźniak et al., 2010). This amount also allowed accurate weighing and quantitative recovery of particulate matter from our small experimental system. An equilibrium time of 48 h was used for our adsorption experiments. Based on our kinetic experiments (data not shown), particle adsorption of these nuclides after 48 h had reached 81%, 95%, 98%, 92% and 100% for ^{210}Pb , ^{234}Th , ^{233}Pa , ^7Be and ^{210}Po , respectively, of their maximum particle sorption after 120 h. The disadvantage of using a longer experimental/equilibrium time is that it would have resulted in more loss of these isotopes onto the reservoir walls, especially for ^7Be and ^{234}Th . Wall-adsorption of these nuclides after 120 h accounted for 4%, 38%, 18%, 26% and 0% of ^{210}Pb , ^{234}Th , ^{233}Pa , ^7Be and ^{210}Po , respectively, of the total amount that adsorbed to particles after 48 h. Therefore, an equilibrium time of 48 h was consistently used for all adsorption experiments. At the end of the experiment, the solution was filtered through 0.2 μm Microsep™ polyethersulfone centrifugal filters (Pall Life Sciences), and the particulate ($>0.2\mu\text{m}$) and dissolved ($<0.2\mu\text{m}$) fractions retained for measurements of radionuclide activity. Before filtration, both filter and filtration tubes were pretreated with ultrafiltered seawater to reduce the tracer adsorption.

Release of tracers adsorbed to container walls was assessed by conducting a 2-day sorption test using solutions with and without the presence of particles (SiO_2 , Sigma-Aldrich® S5631, 0.5–10 μm , 40 mg/l). The acid recoverable tracer from the container walls was usually less than 10% of the total adsorbed tracer. Therefore, the tracer fraction that was lost to container walls was irreversibly lost, and could thus be ignored from the calculations, as it did not participate in the solution reactions any more. This behavior justified using the sum of the measured fractions as the total amounts participating in the reactions that were studied.

2.4. Measurements of radionuclides and their partition coefficients

Activity concentrations of ^{234}Th , ^{233}Pa , ^{210}Pb and ^7Be were measured by gamma counting the 63.5 keV, 312 keV, 46.5 keV and 477.6 keV lines, respectively, on a Canberra ultra-high purity germanium well type detector. The ^{210}Po activity was analyzed by liquid scintillation counting (Beckman Model 8100 Liquid Scintillation Counter). All activities of selected radionuclides were corrected for decay (and ingrowth in case of ^{233}Pa) and normalized to the same geometry for ease of comparison and further evaluation.

Partition coefficients (K_d) between dissolved and particulate phases were determined to quantify the interactions between radionuclides and particles in experimental systems. K_d is defined as:

$$K_d = A_p / (A_d * C_p) \quad (1)$$

where A_p and A_d represents particulate and dissolved activities of radionuclides (Bq/l), respectively, and C_p is the particle concentration (g/ml) (Honeyman and Santschi, 1989). As described before, a small fraction of each radionuclides sorbed to walls appeared to be irreversibly sorbed onto container walls, and therefore, was not considered in the K_d calculations.

2.5. Statistical analysis

The whole data set obtained from OFP particle composition analysis and partition coefficient experiments of all selected radionuclides ($n = 61$ for all 16 variables) is summarized in Appendix 2. A serial statistical analysis was performed on this unique data matrix, using the IBM SPSS software® package.

Two-tailed Pearson Product Moment Correlation analysis was executed to determine the significant correlations between each of two variables. Factor analysis (varimax) was performed to evaluate relationships among the compositional variables and the partition coefficients (K_d), using all samples. All chemical components determined in this study were used except hydroquinone content, due to the limited number of analyses ($n = 30$). In a generalized adsorption/desorption reaction: $C \leftrightarrow X$, where X = concentration of a given species in solid phase (g or mole per gram of solid), and C = concentration of a given species in liquid phase (g or mol per cm^3 of liquid), the equilibrium constant K_d is $K_d = X / C = \exp(-\Delta G_r / (RT))$. $\log K_d$ is proportional to $-\Delta G_r$, which is the Gibbs free energy change of the sorption reaction. Therefore, $\log K_d$ values were used for all statistical analyses to evaluate the possible carrier phases for radionuclides. The adequacy of our data for factor analysis was evaluated by the Kaiser–Meyer–Olkin (KMO) measure of the sampling adequacy method. Factors were extracted by principle component analysis, and rotated by the varimax method with Kaiser Normalization. For Pearson correlation tests, pair-wise deletion was used when there were missing data; and for factor analysis, list-wise deletion was used when there were missing data.

3. Results

3.1. Average composition of the OFP trap particles ($<125\mu\text{m}$)

The organic (organic carbon, proteins, total carbohydrates, uronic acids, hydroquinones and hydroxamate siderophores), and inorganic (Si, Fe, Mn, CaCO_3) compositions of sediment trap samples, and the $\log K_d$ values for radionuclides (^{234}Th , ^{233}Pa , ^{210}Po , ^{210}Pb and ^7Be) are given in Appendix 1 and their averages in Table 1. Our measured average Si, Fe and Mn values for $<125\mu\text{m}$ trap particles are comparable with those for $<1000\mu\text{m}$ particles analyzed by Huang and Conte (2009); and the differences are within 20% or better.

In terms of overall particle composition, CaCO_3 is the most abundant component in OFP samples, ranging from 29.4% to 76.3% (Appendix 1),

Table 1

Averages of $\log K_d$ values of radionuclides, particulate organic and elemental concentrations and the total particle fluxes at three depths at the Oceanic Flux Program (OFP) site off Bermuda.

	Depth					
	500 m (n = 14)		1500 m (n = 22)		3200 m (n = 25)	
	Mean	Std	Mean	Std	Mean	Std
$\log K_d(\text{Th})$	5.08	0.56	5.66	0.53	5.53	0.31
$\log K_d(\text{Pa})$	4.85	0.14	5.28	0.25	5.24	0.19
$\log K_d(\text{Pb})$	3.95	0.32	3.92	0.29	4.07	0.25
$\log K_d(\text{Po})$	5.20	0.21	5.54	0.2	5.66	0.16
$\log K_d(\text{Be})$	4.19	0.24	4.41	0.29	4.44	0.19
Flux $\text{mg/m}^2/\text{d}$	40.3	26.1	33.6	15.0	36.4	15.3
CaCO_3 %	57.3	12.1	63.0	4.9	61.1	3.8
Si %	5.68	1.48	6.21	1.17	6.95	1.03
OC %	11.08	2.69	6.76	0.85	5.03	0.57
TCHO mg/g	82.4	33.1	55.0	19.8	32.6	13.2
Protein mg/g	59.6	14.2	62.5	17.8	45.2	10.1
URA mg/g	53.8	22.2	31.1	10.5	6.57	1.58
HS mg/g	24.5	5.4	30.2	8.1	28.5	6.4
HQ mg/g	1.29	0.46	0.60	0.12	0.47	0.14
Mn mg/g	0.21	0.27	1.32	0.39	1.32	0.27
Fe mg/g	4.55	2.90	6.07	1.40	7.51	1.05

with an average value of 61.0% over the whole water column. The average content of CaCO_3 shows a fairly stable distribution without any decreasing or increasing trends in samples from the three different depths (Table 1). In contrast, the average content of Si, Mn and Fe in the sediment trap samples shows a significant increase with increasing depth (Table 1). For organic components in the OFP samples, total organic carbon (OC) comprised 4.1% to 16.0% of the total weight, showing a significant decrease with depth (Table 1). Similar to OC, the concentrations of TCHO, URA and HQ were relatively high for surface samples and decreased with depth. Particulate HS concentrations, however, were lower in the 500 m-depth samples than in the deeper water column samples (Table 1).

3.2. Partitioning of ^{234}Th , ^{233}Pa , ^{210}Po , ^{210}Pb and ^7Be between dissolved and particulate phases

$\log K_d$ values derived from OFP sinking particulate samples after 2 days equilibration ranged from 4.17 to 7.08 for ^{234}Th , 4.57 to 5.67 for ^{233}Pa , 4.99 to 5.88 for ^{210}Po , 3.32 to 4.60 for ^{210}Pb and 3.73 to 4.81 for ^7Be , respectively (Table 2 and Appendix 1). While it is possible that K_d values would have been higher after longer equilibration times (e.g., Nyffeler et al., 1984), potential problems from colloids generation and wall adsorption limited equilibration times to 2 days.

The average $\log K_d$ values of these radionuclides, 5.5 for ^{234}Th , 5.2 for ^{233}Pa , 5.5 for ^{210}Po , 4.0 for ^{210}Pb , and 4.4 for ^7Be , followed the order of $\text{Po} \geq \text{Th} > \text{Pa} > \text{Be} > \text{Pb}$ in the water–particle partitioning experiments (Table 1). Moreover, $\log K_d$ values of Po, Pa and Be show increasing trends with depth (From here on, we adopt symbol $\log K_d(X, Y, Z)$ to represent $\log K_d$ values of X, Y and Z). The $\log K_d(\text{Th})$ of deep water samples (1500 m and 3200 m) are significantly higher than those of the 500 m samples; however, $\log K_d(\text{Pb})$ shows relatively constant values among three depths (Table 1).

3.3. Effects of particle composition on the partitioning of ^{234}Th , ^{233}Pa , ^{210}Po , ^{210}Pb and ^7Be between dissolved and particulate phases

Relationships among the concentrations of particle components and $\log K_d$ values of radionuclides were obtained as a correlation matrix (Table 3) by applying the Pearson Product Moment Correlation method on all data (Appendix 1). Different components or phases varied in their correlation with the $\log K_d$ values of the radionuclides. We arbitrarily call a weak correlation when the correlation coefficient $\gamma = 0.3\text{--}0.39$, a moderate correlation when $\gamma = 0.4\text{--}0.49$, and a strong correlation

Table 2

Comparisons of $\log K_d$ values among ^{234}Th , ^{233}Pa , ^{210}Po , ^{210}Pb and ^7Be from different aquatic environments.

Nuclides	Study areas	$\log K_d$ range	References	
^{234}Th	OFP	4.17–7.08	This study	
	AESOPS, EqPac, MAB and others ^a	5.59–6.95	Chase et al. (2002)	
	OFP	4.64–6.86	Roberts et al. (2009)	
	Gulf of Mexico	5.22–6.62	Roberts et al. (2009)	
	Controlled experiments			
	SiO_2	3.98	Guo et al. (2002a)	
	CaCO_3	5.60		
	SiO_2	5.90–6.23	Geibert and Usbeck (2004)	
	CaCO_3	5.04–5.18		
	SiO_2	5.54	Roberts et al. (2009)	
^{233}Pa	CaCO_3	5.70		
	OFP	4.57–5.67	This study	
	AESOPS, EqPac, MAB and others ^a	5.34–6.15	Chase et al. (2002)	
	OFP	3.90–7.12	Roberts et al. (2009)	
	Gulf of Mexico	3.96–4.66	Roberts et al. (2009)	
	Controlled experiments			
	SiO_2	5.09	Guo et al. (2002a)	
	CaCO_3	3.68		
	SiO_2	5.60–6.00	Geibert and Usbeck (2004)	
	CaCO_3	5.23–7.79		
^{210}Po	SiO_2	4.39	Roberts et al. (2009)	
	CaCO_3	5.11		
	OFP	4.99–5.88	This study	
	Southern North Sea	4.41–6.01 ^b	Zuo and Eisma (1993)	
	Northwestern Mediterranean Sea	5.08–6.30	Masque et al. (2002)	
	Northwestern Mediterranean margin	3.84–7.06 ^b	Tateda et al. (2003)	
	Controlled experiments	3.02–5.48	Yang et al. (2013)	
	OFP	3.32–4.60	This study	
	^{210}Pb	Southern North Sea	4.34–6.82 ^b	Zuo and Eisma (1993)
		Northwestern Mediterranean Sea	4.56–6.22	Masque et al. (2002)
Gulf of Mexico		5.08–6.89	Baskaran and Santschi (2002)	
Northwestern Mediterranean margin		4.23–6.99 ^b	Tateda et al. (2003)	
Controlled experiments		3.22–6.49	Yang et al. (2013)	
OFP		3.73–4.81	This study	
Sabine-Neches estuary, Texas		3.18–4.94	Baskaran et al. (1997)	
Loire estuary		4.57–4.91	Ciffroy et al. (2003)	
Tampa Bay, Florida		3.00–5.19 ^b	Baskaran and Swarzenski (2007)	
Controlled experiments		3.57–4.65	Yang et al. (2013)	

^a SW Pacific sector of the Southern Ocean (AESOPS), the equatorial Pacific (EqPac) and the Mid Atlantic Bight (MAB).

^b The $\log K_d$ values were calculated according to the reported dissolved, and particulate activities of radionuclides, and the concentrations of suspended particulate matter.

when $\gamma \geq 0.5$ in the following discussion using this approach. The most abundant component CaCO_3 is moderately correlated with $\log K_d(\text{Th})$ and weakly with $\log K_d(\text{Be})$; Mn is strongly correlated with $\log K_d(\text{Po}, \text{Pa})$ and weakly with $\log K_d(\text{Th}, \text{Be})$; Fe is strongly correlated to $\log K_d(\text{Po})$; and HS is strongly correlated with $\log K_d(\text{Po})$ and moderately with $\log K_d(\text{Pa})$ (Table 3). In terms of the bulk organic material, OC shows a moderate to strong negative correlation with $\log K_d(\text{Th}, \text{Po}, \text{Pa})$ and a weak negative correlation with $\log K_d(\text{Be})$. Among all radionuclides, only $\log K_d(\text{Pb})$ shows a weak negative correlation with protein.

Factor analysis (varimax) was used to further explore the effects of particle composition on radionuclide partitioning and find the most likely carrier phase(s) for radionuclide binding in the sediment trap samples. The KMO values obtained were with a high significance level ($p < 0.001$). Four factors with eigenvalues greater than one were extracted.

With all samples analyzed, four extracted factors explained 70.9% of the total variance present in the original data set (Table 4). Factor loadings (fl) of $-0.4 \geq \text{fl} \geq 0.4$ are considered here to be significant (bold numbers in Table 4). The factor loadings of variables on factors 1 to 4

Table 3

R-values for each two crossed factors by 2-tailed Pearson Product Moment Correlation (pair-wise deletion for missing data).

	logK _d (Th)	logK _d (Pa)	logK _d (Pb)	logK _d (Po)	logK _d (Be)	CaCO ₃	OC	Si	Mn	Fe	TCHO	Protein	URA	HS	HQ
logK _d (Th)	1.00	0.26	-0.07	0.25	0.26	0.45**	-0.44**	-0.08	0.38**	0.05	-0.39**	-0.05	-0.39**	0.15	-0.54**
logK _d (Pa)	0.26	1.00	0.03	0.57**	0.08	0.02	-0.48**	0.26	0.57**	0.28	-0.45**	0.04	-0.38**	0.40**	-0.46
logK _d (Pb)	-0.07	0.03	1.00	0.13	-0.07	-0.23	-0.15	0.13	0.15	0.24	0.03	-0.30	-0.10	-0.17	-0.01
logK _d (Po)	0.25	0.57**	0.13	1.00	0.16	0.06	-0.57**	0.13	0.69**	0.51**	-0.57**	0.03	-0.50**	0.51**	-0.57**
logK _d (Be)	0.26	0.08	-0.07	0.16	1.00	0.36**	-0.33	0.27	0.34	0.16	-0.26	-0.33**	-0.37**	0.00	-0.60**
CaCO ₃	0.45**	0.02	-0.23	0.06	0.36**	1.00	-0.48**	-0.35**	0.15	-0.47**	-0.39**	0.07	-0.42**	0.08	-0.50**
OC	-0.44**	-0.48**	-0.15	-0.57**	-0.33	-0.48**	1.00	-0.21	-0.70**	-0.29	0.74**	0.29	0.79**	-0.17	0.79**
Si	-0.08	0.26	0.13	0.13	0.27	-0.35**	-0.21	1.00	0.24	0.43**	-0.03	-0.20	-0.18	0.02	-0.26
Mn	0.38**	0.57**	0.15	0.69**	0.34	0.15	-0.70**	0.24	1.00	0.59**	-0.55**	-0.23	-0.62**	0.34**	-0.70**
Fe	0.05	0.28	0.24	0.51**	0.16	-0.47**	-0.29	0.43**	0.59**	1.00	-0.18	-0.29	-0.40**	0.23	0.05
TCHO	-0.39**	-0.45**	0.03	-0.57**	-0.26	-0.39**	0.74**	-0.03	-0.55**	-0.18	1.00	0.19	0.73**	-0.37**	0.72**
Protein	-0.05	0.04	-0.30	0.03	-0.33**	0.07	0.29	-0.20	-0.23	-0.29	0.19	1.00	0.47**	0.18	0.12
URA	-0.39**	-0.38**	-0.10	-0.50**	-0.37**	-0.42**	0.79**	-0.18	-0.62**	-0.40**	0.73**	0.47**	1.00	-0.17	0.68**
HS	0.15	0.40**	-0.17	0.51**	0.00	0.08	-0.17	0.02	0.34**	0.23	-0.37**	0.18	-0.17	1.00	-0.17
HQ	-0.54**	-0.46	-0.01	-0.57**	-0.60**	-0.50**	0.79**	-0.26	-0.70**	0.05	0.72**	0.12	0.68**	-0.17	1.00

(Bold value with ** denotes correlations significance level <0.01).

(F1 to F4) are plotted in Fig. 1. For clarity, some variables are omitted in Fig. 1 when their factor loadings were $-0.4 \leq f_i \leq 0.4$ in the two plotted factors. In Fig. 1, variables within one dotted oval have significant correlation (either $\gamma \geq 0.4$ or $\gamma \leq -0.4$) between any pair of them in the correlation matrix (Table 3). Two variables connected by straight lines are also significantly correlated. According to Fig. 1a, factor 1 (F1) is represented by logK_d(Po, Pa), HS, Mn and Fe. However, HS alone does not correlate significantly with Mn and Fe. The negative factor 1 (-F1) is represented by TCHO, OC, and URA. Members of F1 and -F1 groups are inversely correlated. F2 is represented by logK_d(Be) and Si. However, the correlation coefficient between Si and logK_d(Be) pair is very low ($\gamma = 0.27$). Instead, Si is moderately correlated with Fe ($\gamma = 0.43$). -F2 represents protein which is partially correlated with URA. F3 is represented by carbonate, particle flux and logK_d(Th), and -F3 by Si and OC (Fig. 1b). The high correlation between carbonate and particle flux implies that the observed seasonal variation of particle flux is mainly caused by the change in the surface production rate of carbonate in the study area. Si and OC may have a dilution effect on the content of carbonate in the trap sediments. F4 is represented by protein, URA and partially by OC, and -F4 by logK_d(Pb) alone. Also, it should be mentioned that in Table 3, HS had a F4 loading of 0.4 but is not shown in Fig. 1b, because it is likely an artifact caused by the varimax operation. According to the correlation matrix (Table 3), HS does not correlate with protein, URA, and OC, nor negatively with logK_d(Pb).

Table 4Rotated structure matrix derived from the covariance matrix with logK_d of selected radionuclides with data from all three depths.

	Component			
	1	2	3	4
% of variance	36.46	13.49	13.03	7.89
logK _d (Po)	0.90	0.07	-0.06	-0.11
logK _d (Pa)	0.74	-0.04	-0.15	0.10
Mn	0.72	0.36	-0.11	-0.29
HS	0.67	-0.11	-0.08	0.40
Fe	0.64	0.43	-0.36	-0.34
logK _d (Th)	0.34	0.07	0.54	-0.14
Si	0.24	0.61	-0.40	0.04
Protein	0.08	-0.65	0.08	0.51
logK _d (Be)	0.07	0.80	0.21	0.19
logK _d (Pb)	0.06	-0.07	-0.11	-0.82
CaCO ₃	-0.07	0.03	0.91	0.18
Flux	-0.32	-0.06	0.76	0.08
URA	-0.50	-0.56	-0.13	0.43
OC	-0.62	-0.41	-0.41	0.38
TCHO	-0.63	-0.31	-0.19	0.09

(Bold and italic value denotes loadings at a significance level of ± 0.4 . Numbers with underline denotes their significance level of $+0.4$).

In complement to the results of the factor analysis, Figs. 2 and 3 provide the x-y correlation plots of the concentrations or ratios of selected variables in sediment trap samples to illustrate in detail the variation patterns of variables among the samples obtained at three different sampling depths (500 m, 1500 m and 3200 m). Relevant features of those figures are highlighted in the following discussion section.

4. Discussion

4.1. Hydroxamate siderophores in marine particulate organic materials

So far, very little attention has been paid to the presence of siderophores in particulate organic matter (suspended or sinking particles $>0.2 \mu\text{m}$) in the marine environment. Even less attention has been paid to the molecular-level mechanisms regulating the interactions between natural radionuclides and siderophores. Surprisingly, strongly Fe(III) complexing hydroxamate siderophores (HS) were found to contribute a relatively high percentage (1.57 to 5.25%) of the total particulate weight in the sediment trap samples (Appendix 1) but catechol siderophores were below the detection limit. The catechol siderophores, which are also known to form very stable complexes with Fe are also very efficient in dissolving Fe bearing minerals (Albrecht-Gary and Crumbliss, 1998). Furthermore, they can shift the redox potential to such a low region that it does not allow biological reductants to reduce the complex (Albrecht-Gary and Crumbliss, 1998). However, the reasons why we did not detect any particulate catechol siderophores but find high concentration of HS in OFP particles are still unclear. Further molecular level structural analysis of siderophore moieties in different extractant solutions would be needed to resolve these questions.

The average HS flux at OFP site off Bermuda was about $1 \text{ mg-C m}^{-2} \text{ day}^{-1}$, staying relatively constant over the 3500 m water column (data derived from Appendix 1, the fluxes of various parameters = total particle flux \times concentrations of various parameters in particles). Compared to the average gross primary productivity in the Sargasso Sea off Bermuda ($160 \text{ g-C m}^{-2} \text{ yr}^{-1}$, or $440 \text{ mg-C m}^{-2} \text{ day}^{-1}$; Menzel and Ryther, 1959), this flux is about 0.23% of the primary productivity, or compared to an organic carbon downward export flux of $9 \text{ g-C m}^{-2} \text{ yr}^{-1}$, or $25 \text{ mg-C m}^{-2} \text{ day}^{-1}$ (G. Kim et al., 2003), the HS flux is about 4% of the average OC flux. Moreover, the HS flux remained fairly constant over all depths, suggesting that HS is likely a refractory organic component, at least on the time scale of particle sinking. This is also supported by FA results in F1 loadings, where HS is shown to be negatively correlated with OC, TCHO and URA. As shown in Fig. 2b, HS-C/OC ratio is relatively high for samples from 1500 m and 3200 m depths as compared with those from 500 m. Fig. 2c to e show systematic decreases of TCHO, URA and HQ concentrations with sampling depth,

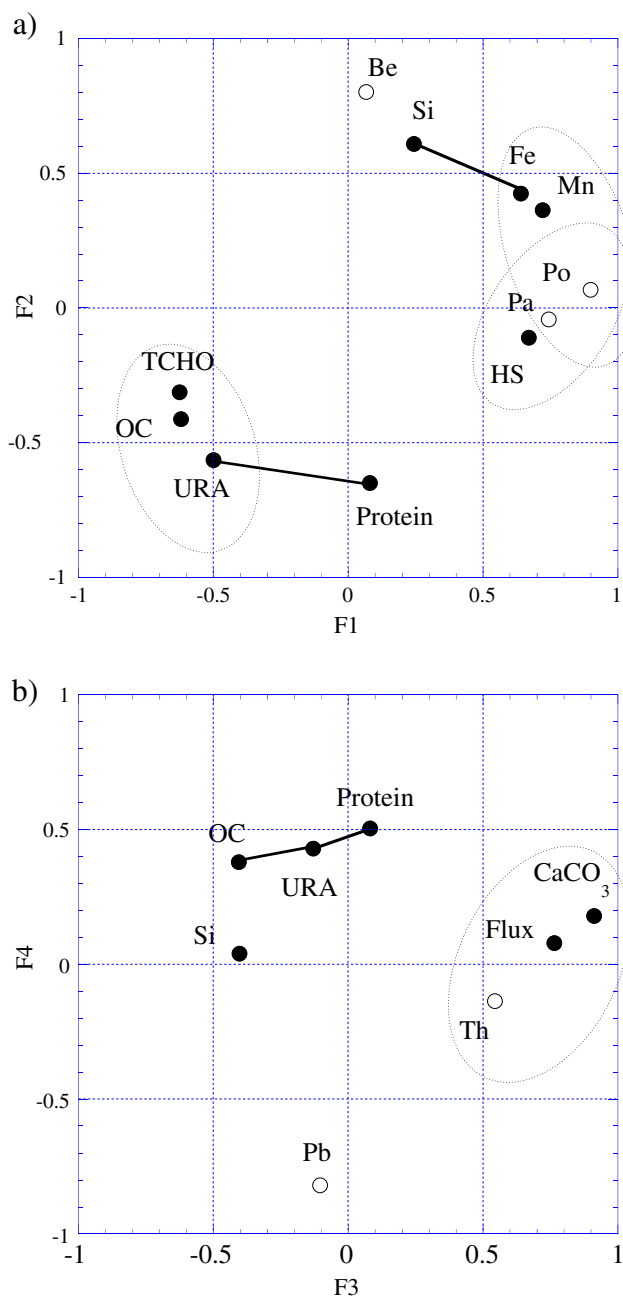


Fig. 1. Graphic representation of factor analysis (FA) carried out with all three depths samples (open circle: radionuclides; filled circle: possible carrier phases/proxies). a) Distribution of factors according to their loadings of F1 and F2; b) distribution of factors according to their loadings of F3 and F4.

indicating their labile nature. The stability of protein probably lies between HS and URA (Fig. 2f).

The contribution of HS to the particulate organic carbon (POC) flux at depth is below that of the uncharacterized organic carbon fraction in the same depth range. Lee et al. (2004) found that the percentage of uncharacterized carbon in the particle flux in the equatorial Pacific Ocean at 105 m, 1000 m and in >3500 m was ~20%, 70% and >70%, respectively. Similarly, (Hirose and Tanoue, 2001) found that approximately 40% of deep POC at 2000-m depth in the North Pacific Ocean and Bering Sea was refractory POC, with the strong organic ligand (SOL) to POC ratio in the per mil range. Results from Hirose (1995) furthermore suggest that the Th complexation capacity of suspended particulates in the surface ocean is about 10 nM. Given that suspended

particle concentrations are of the order of 100 µg/l, the estimated strong organic Th ligand (SOL) concentrations can be in the order of 100 µmol/g. Such a value is similar to the HS and Fe concentrations measured in our OFP subsamples. A later study from the same group (Hirose and Tanoue, 2001), suggested that the main source of the SOL is marine bacteria, because the concentration of the chelator in phytoplankton and zooplankton is more than one order of magnitude lower than that of bacteria. It is quite likely that SOL or uncharacterized carbon is mainly composed of HS molecules. Further studies are needed to confirm this hypothesis.

The relatively high ratio of siderophore moieties to OC in the deep water particles (Fig. 2b) may indicate that siderophore moieties become more stable through Fe(III) chelation. Available chemical speciation data of particulate iron from the oceanic literature using EXAFS/XANES and microXAS did not clearly differentiate organo-Fe from inorganic Fe (Lam et al., 2002; Duckworth et al., 2008). These methods, however, documents that the majority of open ocean particulate iron is trivalent Fe (Lam et al., 2012), even though a number of researchers also documented Fe(II) phases (e.g., Fe-sulfides) near upwelling sites or hydrothermal plumes (Lam et al., 2012; Toner et al., 2012). However, at the OFP site, one could expect that most of the Fe would be organo-Fe(III) (hydroxamate-bound Fe), as a significant fraction of OC is composed of hydroxamate-C. Nonetheless, our results would need to be confirmed by other methods, e.g., by EXAFS/XANES and/or micro-XAS.

In Huang and Conte (2009), some direct evidence for the relative partitioning of Fe with organic matter and inorganic materials is presented. These authors reported a crustal enrichment factor of 1.3–1.4 for Fe in OFP sediment trap particles, suggesting some enrichment of Fe in organic phases. Similarly, the relative factor loadings of Fe from PMF (Positive Matrix Factorization) analysis indicated that at 500 m depth ~20% of the Fe is associated with organic matter and 20% with oxy-hydroxides; at 1500 and 3200 m Fe is more evenly distributed among possible carrier phases, including shale particles.

Besides, it is possible that physicochemical properties of siderophores are changing with depth, due to bacterial reworking (Jiao et al., 2010), change in relative hydrophobicity, and subsequent chemical modifications (cross-linking) of particulate organic matter. Thus, siderophores may play a more important role in the biogeochemical cycle of trace metals (e.g., Fe) and natural radionuclides (e.g., Po and Pa, in this study) than previously thought. There is also a direct evidence from flow injection electrospray ionization mass spectrometry, which showed that the cation Th(IV) can replace Fe(III) to form a strong and soluble Th-hydroxamate siderophores complex in terrestrial environments (Keith-Roach et al., 2005). The implication is that hydroxamate siderophores can enhance the mobility of actinides(IV) in such environments.

Laboratory experiments have shown that, after deprotonation, monohydroxamic acids, such as acetohydroxamic acids $\text{CH}_3\text{CONHOH} = \text{AHA}$ (the standard used to determine the HS concentration in this study), act as bidentate ligands to form octahedral complexes with Fe(III). Fe(III) is coordinated through two ketonic oxygen atoms of the $-\text{CONHO}-$ group, which exhibit octahedral configuration both in the solid state and in solution (Kurzak et al., 1992). This is confirmed by X-ray diffraction studies (Brown et al., 1979). In addition, the stabilities of the chelating compound increases with increasing size of the substituent of R in the monohydroxamic acids, such as R-COHNHOH (Brown et al., 1979). In a Fe(III)-hydroxamate complex, at least three units of monohydroxamic acids are required for Fe chelation. In OFP particles, the HS/Fe molar ratio averages 3.92 (ranging from 1.54 to 14.86, derived from Appendix 1), indicating sufficient hydroxamate binding sites for Fe and other metals such as Pa and Po.

According to another structural study of the marine hydroxamate siderophore exochelin MS (the extracellular siderophore from *Mycobacterium smegmatis*, Dhungana et al., 2004), there are seven protonation sites for metal binding, one on a carboxylic acid, three on hydroxamate sites, and three on primary amine groups. The binding of

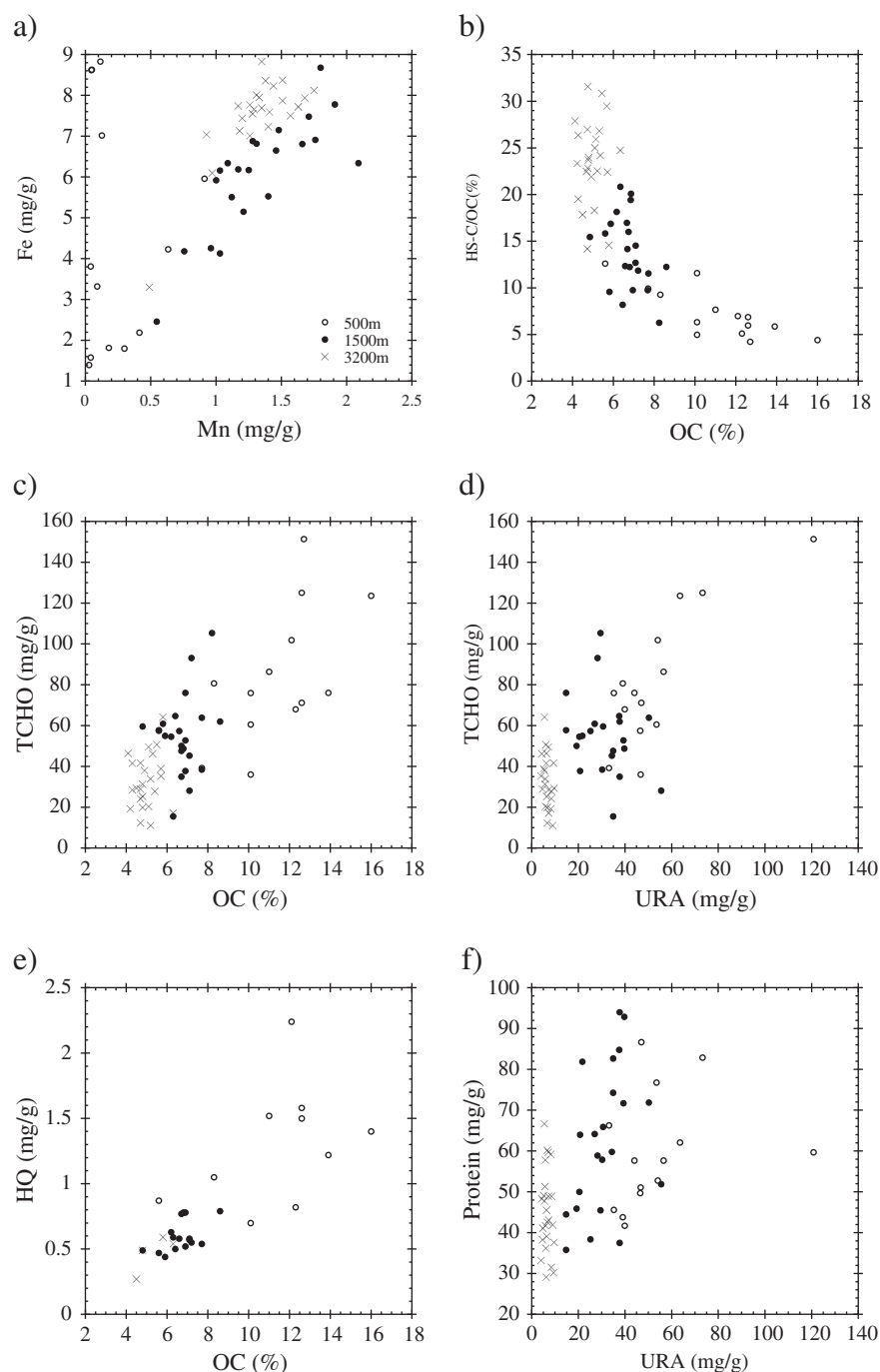


Fig. 2. Correlations of particulate concentration (in wt/wt unit) of a) Mn with Fe; b) OC with HS-C/OC; c) OC with TCHO; d) URA with TCHO; e) OC with HQ; f) URA with protein; in three different depths.

radionuclides with natural hydroxamate siderophores might also form a similar configuration. As a consequence of the heterogeneity of the binding sites, the isoelectric point, pH_{IEF} , of any extracted radionuclide-binding molecule would be expected to show different pH_{IEF} patterns due to the different pK_a values of different binding sites, as was found by Chuang et al. (2013b).

4.2. Effects of particle composition on the scavenging and fractionation of radionuclides

K_d values comparable to ours can be found in the literature (e.g., Zuo and Eisma, 1993; Baskaran et al., 1997; Baskaran and Santschi, 2002; Chase et al., 2002; Guo et al., 2002a; Masque et al., 2002; Ciffroy et al.,

2003; Tateda et al., 2003; Geibert and Usbeck, 2004; Baskaran and Swarzenski, 2007; Roberts et al., 2009; Yang et al., 2013), ranging from 10^3 to 10^7 for different radionuclides in marine environments (Table 2). However, because of the well documented particle-concentration effect (Li et al., 1984; Honeyman and Santschi, 1989) on $\log K_d$ for many of these radionuclides, and since we used a particle concentration of 10 mg/l, typical for near-shore waters (Baskaran and Santschi, 1993; Woźniak et al., 2010), K_d values can be higher at lower particle concentration such as those occurring in the open ocean (typically less than 1 mg/l; Guo et al., 1997).

The observed close association among Mn, Fe, HS, and $\log K_d$ (Po, Pa) (Fig. 1, Tables 3 and 4) in the trap samples may be explained by the following coupled processes: Mn(II)-oxidizing bacteria are encoded by

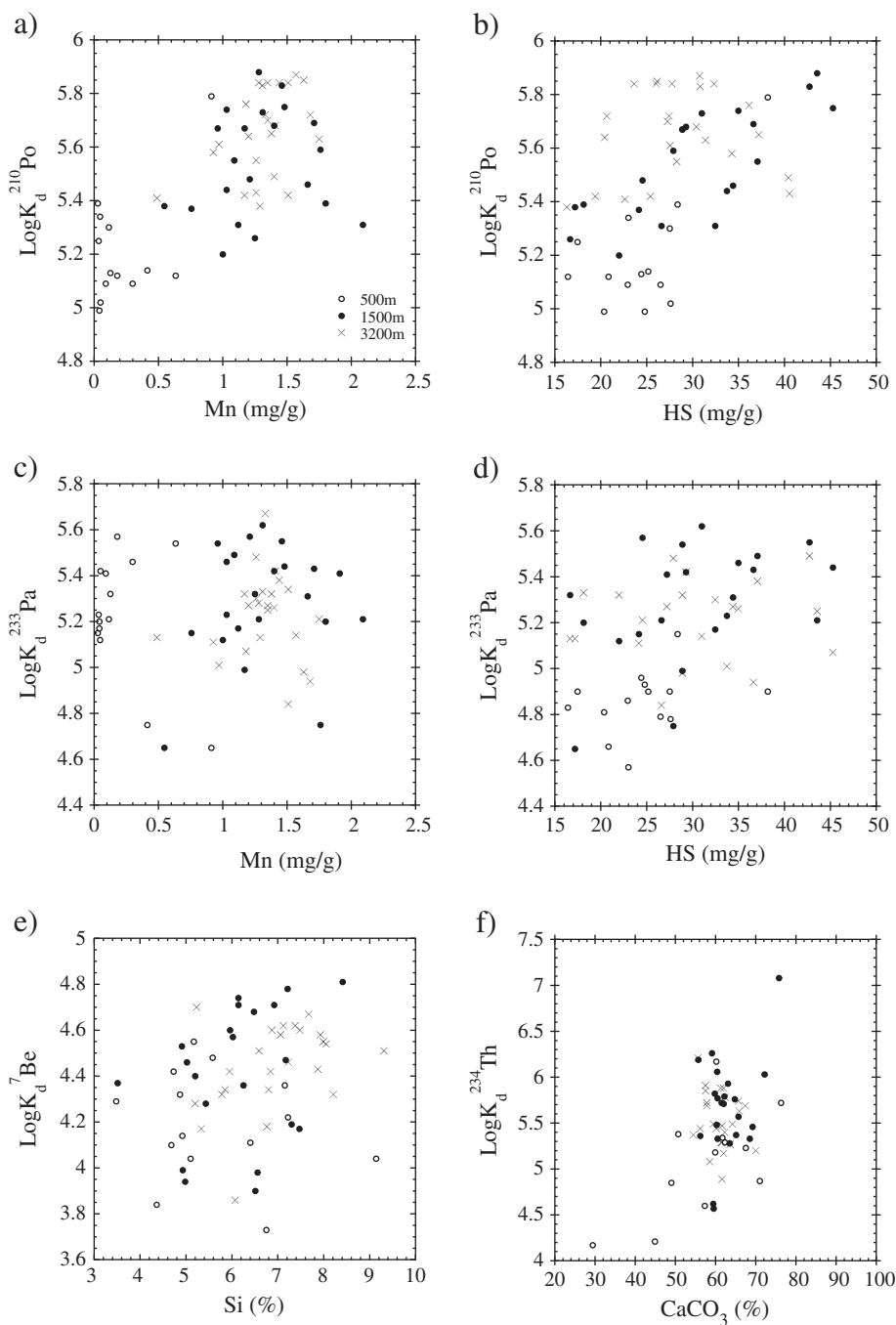


Fig. 3. Correlations of a) particulate Mn concentration with $\text{log}K_d^{210}\text{Po}$; b) particulate HS concentration with $\text{log}K_d^{210}\text{Po}$; c) particulate Mn concentration with $\text{log}K_d^{233}\text{Pa}$; d) particulate HS concentration with $\text{log}K_d^{233}\text{Pa}$; e) particulate Si concentration with $\text{log}K_d^{7}\text{Be}$; f) particulate CaCO_3 concentration with $\text{log}K_d^{234}\text{Th}$; in three different depths.

specific oxidase genes to oxidize Mn(II) and Mn(III) (Geszvain et al., 2013). HS forms a strong complex with Mn(III) and stabilizes Mn(III), thus enhances the oxidation of Mn(II) to Mn(III) and MnO_2 (Spiro et al., 2009; Geszvain et al., 2011; Madison et al., 2011; Harrington et al., 2012). Therefore, Po and Pa may be incorporated into MnO_2 (Fig. 3a and c), and/or taken up by HS through ion exchange with Fe(III) and Mn(III) (Fig. 3b and d). Another possible explanation is as follows: As shown in Fig. 2a, most of the samples from 500 m have very low Mn content (<0.2 mg/g) but have a wide range in Fe content (1 to 9 mg/g). In contrast, samples from 1500 m and 3200 m are high in Mn content but the range in Fe content is still similar to that of 500 m. Meanwhile Mn and Fe contents are highly correlated. It might

be possible then that the oxidation of Mn(II) to Mn(III) and to MnO_2 could also be catalyzed by Fe containing minerals without invoking HS as facilitator. Which of these coupled processes are realized in the ocean is not known, even though one might expect that microbial involvement is more likely.

Using the average compositions of OFP sediment trap samples given by Huang and Conte (2009), we roughly estimate the relative abundance of possible carrier phases for radionuclides at different depths. By assuming that all Al in samples is contributed by shale particles (alumino-silicates), the contributions from shale for other elements are calculated and subtracted from the total to obtain the net as shown in Appendix 2. Using the data in the net columns, OC is converted

to dry organic matter, Fe to Fe₂O₃, Mn to MnO₂, Ca to CaCO₃, and Si to SiO₂(opal). The shale content in samples is estimated from the ratio of Al contents in the sample and the global average shale (Li, 2000). The results are summarized in Table 5 (by normalizing the total wt.% as 100%). The contents of shale particles, opal, Mn–Fe oxides increase with depth, while the content of organic matter decreases drastically, and that of carbonate remains nearly constant (Table 5). In comparison, logK_d(Th, Po, Pa, Be) values increase with depth (Table 1), while logK_d(Pb) remains nearly constant. Interestingly, about 10–12% of Fe is present as iron oxides; 75–88% Mn as manganese oxides, and 62–69% of Si as opal; while the remaining fractions are all contributed by shale particles in the OFP samples (Appendix 2).

It is not surprising then that OC is not a good predictor for radionuclide scavenging, even though, as our data suggest, sorption to biopolymers likely controls the extent of scavenging. This is due to the fact that these biopolymers are minor components in the particle flux, and co-produced with biogenic silica and CaCO₃ shells, thus hiding their role when one only determines major components in the sinking or suspended particle assemblage. From F2 and F3 factor loadings (Table 4), it is apparent that CaCO₃ and opal (Si) might be good predictors of scavenging of selective radionuclides (CaCO₃ for Th and SiO₂ for Be), as also suggested by Chase et al. (2002). However, in order to get 10% of a dissolved radionuclide to adsorb onto suspended or sinking particles, this would require logK_d values of 6 or higher for that particle component in the ocean. Typical logK_d values for pure CaCO₃ and SiO₂ phases are, however, only 3 to 5 for these radionuclides (Table 2, and summary in Roberts et al., 2009). In addition, our unpublished results (Chuang et al., 2013a,b) show that acid-cleaned silica frustules from diatom *Phaeodactylum tricornutum* give logK_d values similar to commercially available pure SiO₂ for five different radionuclides (²³⁴Th, ²¹⁰Pb, ²³³Pa, ⁷Be and ²¹⁰Po), and are 1–2 orders of magnitude lower than those of untreated whole plankton cells, regardless if cells contained biogenic SiO₂ shells or not.

Though both logK_d(Th) and CaCO₃ are high in F3 loadings (Fig. 1b, Table 4), they are only moderately correlated ($\gamma = 0.45$) (Table 3). As shown in Fig. 3f, if one takes out two extreme low points and one high point, the apparent correlation between logK_d(Th) and CaCO₃ content would just disappear. The implication likely is that Th(IV) is evenly distributed to multiple binding moieties on well-documented organic coatings of the sinking particles. Interactive effects between mineral phases and associated biopolymers are thus strongly suggested by our data, a result that would require further study.

Well designed cross- and inter-calibration experiments of different spectrophotometric methods may resolve the observed apparent correlations among CaCO₃, percentage of total carbohydrates-C in total organic carbon (TCHO-C/C%) and logK_d values of Th and Pa found by Roberts et al. (2009). These authors suggested that the carbohydrate content could be used as a proxy parameter for the presence of the strongly chelating compounds or functional groups, since pure carbohydrates are not considered to be effective sorbents for actinides. In our calibration study, the TCHO concentration measured by the TPTZ method was also linearly correlated with AHA (standard for HS

determination) concentration from 0 to 500 mM, suggesting that the correlation observed by Roberts et al. (2009) could also have resulted from the contribution of hydroxamates in the particle samples to the total polysaccharides pool.

Overall, all selected radionuclides, except Pb, showed specific carrier phase(s) in the sorption experiments. These radionuclides are all A-type metals, except for Pb, which is a B-type metal that is expected to prefer to bind to sulfur-containing sites on organic ligands rather than to oxygen-sites. As a consequence of the addition of ultra-high purity HgCl₂ (200 mg/l) preservative in the trap cup brine that arrests biological degradation during sample collection, the sulfur-binding sites on those organic ligands in the particles might all have been occupied by Hg²⁺, another B-type metal. Hence, carrier phase(s) for Pb are not resolved with our approach, and thus, remain uncertain. And this might have also led to relatively lower K_d values of Pb in this study compared with values found in the literatures (Table 2).

4.3. Postulated binding mechanisms

In natural systems, Fe(III) has to compete not only with protons for the siderophore binding sites, but also with other metal ions having similarly strong binding energy. Binding energies for various natural metal ions are dependent on charge, Lewis acidity (hardness), size, d-electron configuration and electronegativity (Albrecht-Gary and Crumbliss, 1998), as well as the ionic potential (z/r) or ionization energy of the binding ions (Iz) (Li, 1991). The special Fe–HS binding structure reflects all these properties, leading to the high binding energy of Fe and high propensity for mobilization by siderophores. From the observed correlations and chemical considerations, we propose that Po(IV) and Pa(IV) are bound to siderophores by replacing Fe(III) with these four-valent ions, which have similar ionic potential (z/r) or ionization energy (Iz). In seawater, the most common oxidation state for Po is indeed the particle-reactive IV state (Hussain et al., 1995).

Some radionuclides have more than one possible oxidation state in natural waters. For example, Pa, its predominant form in seawater is likely Pa(V) (Choppin, 1983), which is more soluble and sorbs to particle surfaces to a lower extent than its four-valent counterpart, Pa(IV), in broad analogy to Pu and Np. Thus, it is likely that Pa(V) must first be reduced to Pa(IV) before adsorption can take place, as has been observed for Np(IV), which is reduced by humic substances in natural waters (Zeh et al., 1999). According to the redox potentials listed in Ahrlund et al. (1973), Pa should more easily be reduced from V to IV state than Pu and Np from V to IV. The redox potential for Pa(V → IV) reduction is 0.29 V in 6 M HCl, while that of Pu in 1 M HClO₄ is given as –1.17 V, and that of Np as –0.74 V. Since hydroquinones, commonly present in humic substances (e.g., Kalmykov et al., 2008, and references therein), have been documented to reduce Pu and Np to their IV state (Zeh et al., 1999; Kalmykov et al., 2008), one could expect that the same should happen to Pa. While Marquardt et al. (2004) have documented the lability and propensity to oxidation of Pa(IV) in pure, highly acidic solutions (but not at neutral pH), they also documented that Pa(IV) is forming very strong complexes to common ligands that could be expected to stabilize the IV oxidation state at neutral pH.

logK_d(Be) is only weakly correlated with Ca ($\gamma = 0.36$) and Mn ($\gamma = 0.34$), and very weakly with Si ($\gamma = 0.27$) and Fe ($\gamma = 0.16$) (Table 3). The apparent association between log K_d(Be), Si and Fe shown in Fig. 1a and Table 4 could again be an artifact of varimax operation. Thus, Be is likely evenly distributed among different carriers. As mentioned before, about 62 to 69% of Si is in the form of opal and the rest in shale. While the Si–OH group on pure silica surfaces is a relatively weak ligand, with a seawater logK_d value for metal ions of only 3 to 5 (Schindler, 1975; Schindler et al., 1976; Schindler and Stumm, 1987; Stumm and Morgan, 1996; e.g., Guo et al., 2002b; Santschi et al., 2006; Roberts et al., 2009), biogenic silica surface appears to form stronger

Table 5
Concentration of selected elements in their estimated forms.

	wt.% in total particles		
	500 m	1500 m	3200 m
Organic matter	32.9	15.4	10.9
Silicate	4.7	11.7	15.9
Opal	6.3	12.8	15.5
Carbonate	56.0	59.9	57.4
MnO ₂	0.02	0.12	0.14
Fe ₂ O ₃	0.03	0.09	0.15
Total	100.0	100.0	100.0

bonds to Be and other metals (e.g., Rutgers van der Loeff and Berger, 1993; Chase et al., 2002; Moran et al., 2002; Scholten et al., 2005; Kretschmer et al., 2011). This stronger bonding could likely be due to the inclusions of templating organic residues, e.g., silaffins (Kröger et al., 2002; Poulsen et al., 2003; Wieneke et al., 2011). Thus, the apparent association between Be and Si could also be considered as a contribution from the binding of a specific organic phase embedded onto the biogenic silica as well as on carbonate shells. Further isolation and identification of the organic molecules/compounds are needed to confirm such an organic binding phase and the potential binding mechanisms.

5. Conclusions

Hydroxamate siderophores (HS) appear to be a main component of recalcitrant organic carbon in the sinking particles and to play an important role in the fractionation and scavenging of Po and Pa in the water column. Based on our results, we propose the following mechanism: Mn(II)-oxidizing bacteria are encoded by specific oxidase genes to oxidize Mn(II) to Mn(III) and to MnO₂. The function of HS is to form strong HS–Fe(III)–Mn(III) complexes to also stabilize Mn(III). The radionuclides of Po and Pa may be directly incorporated into MnO₂, and/or taken up by HS through exchange with Fe(III) and Mn(III) in their 4-valent states. It is also possible that the oxidation of Mn(II) to Mn(III) and to MnO₂ could be catalyzed by Fe containing minerals

without invoking HS as facilitator. However, microbial involvement is more likely. The apparent associations between Si and logK_d(Be) and between CaCO₃ and logK_d(Th) in factor analysis are likely artifacts. The radionuclides of Be and Th are probably evenly distributed among the different major mineral carrier phases, many of which are covered by various biopolymers. This close association between carrier phases and associated biopolymers may obscure the direct bonding of radionuclide to organic biopolymers.

The finding that hydroxamate siderophores (HS) are likely important carriers for some radionuclides warrants a more in-depth evaluation of organic carrier phases at the molecular level, as previously carried out for other radionuclides (e.g., ^{239,240}Pu and ^{127,129}I) (Xu et al., 2008, 2013). Unequivocal identification of the functionalities and binding selectivities of those radionuclides' carrier phases are needed for better data interpretation and understanding of biogeochemical cycles of carbon, iron and natural radionuclides. This information would also be crucial if we are to construct better radioisotopes-based models of the carbon flux and particle dynamics in the ocean.

Acknowledgments

This work was supported by grants from the NSF (OCE#0851191 to P.H.S. and #0850957 to L.G.) and Texas A&M University.

Appendix 1. logK_d values for Th, Pa, Pb, Po and Be, as well as chemical composition of the <125 μm fraction of OFP sediment trap samples

Sample ID	Year	Mid sampling date	Depth (m)	Flux (mg/m ² /d)	CaCO ₃ (%)	Si (%)	OC (%)	TCHO (mg/g)	Protein (mg/g)	URA (mg/g)	HS (mg/g)	HQ (mg/g)	Mn (mg/g)	Fe (mg/g)	logK _d (Th)	logK _d (Pa)	logK _d (Pb)	logK _d (Po)	logK _d (Be)
% 4/05-5	2005	2/8	500	30.3	62.3	4.92	10.1	36.1	51.1	46.7	16.4	–	0.179	1.82	5.29	4.83	3.32	5.12	4.14
% 4/05-6	2005	2/22	500	51.7	61.7	5.17	10.1	76.0	45.6	35.2	20.8	–	0.634	4.23	5.34	4.66	4.07	5.12	4.55
% 4/05-7	2005	3/7	500	67.0	67.5	4.68	8.3	80.7	43.8	39.0	25.2	1.05	0.413	2.19	5.23	4.90	4.12	5.14	4.10
% 4/05-8	2005	3/21	500	100.4	76.3	3.48	5.6	57.5	49.7	46.5	22.9	0.87	0.298	1.80	5.72	4.86	4.19	5.09	4.29
% 8/05-1	2005	4/8	500	38.5	57.3	4.36	12.6	71.2	86.7	47.0	28.4	1.50	0.029	1.40	4.60	5.15	4.28	5.39	3.84
% 11/05-4	2005	9/22	500	24.0	60.2	4.73	10.1	60.6	76.8	53.5	38.2	0.70	0.911	5.96	6.17	4.90	–	5.79	4.42
% 4/06-5	2006	1/26	500	58.1	54.5	6.40	12.1	101.9	52.8	54.0	27.6	2.24	0.049	8.63	–	4.78	4.08	5.02	4.11
% 4/06-7	2006	2/27	500	56.6	59.9	4.87	13.9	76.1	57.7	44.0	26.5	1.22	0.090	3.32	5.18	4.79	3.41	5.09	4.32
% 4/06-10	2006	4/13	500	59.4	71.0	7.22	7.7	39.3	66.3	33.1	24.8	–	0.041	1.58	4.87	4.93	3.72	4.99	4.22
% 8/06-3	2006	5/31	500	21.5	50.7	7.15	12.3	68.0	41.7	39.9	20.4	0.82	0.041	3.81	5.38	4.81	3.98	4.99	4.36
% 8/06-5	2006	7/1	500	11.5	29.4	9.14	12.7	151.4	59.7	120.8	17.5	–	0.035	–	4.17	4.90	4.30	5.25	4.04
% 8/06-6	2006	7/17	500	11.1	–	5.58	16.0	123.6	62.1	63.6	23.0	1.40	0.045	8.62	5.04	4.57	3.79	5.34	4.48
% 12/06-2	2006	9/18	500	16.4	44.9	6.75	12.6	125.1	82.9	73.2	24.4	1.58	0.126	7.02	4.21	4.96	4.14	5.13	3.73
% 12/06-3	2006	10/3	500	18.4	49.0	5.10	11.0	86.4	57.7	56.5	27.5	1.52	0.114	8.83	4.85	4.90	–	5.3	4.04
% 4/05-4	2005	1/25	1500	24.7	62.2	6.48	7.7	38.5	57.9	30.2	24.5	0.54	1.21	5.15	5.79	5.57	4.02	5.48	4.68
% 4/05-5	2005	2/8	1500	46.7	64.8	4.93	7.7	63.9	71.9	50.2	28.9	–	0.96	4.26	5.76	5.54	4.01	5.67	3.99
% 4/05-6	2005	2/22	1500	47.1	69.2	6.14	7.2	93.2	58.9	28.2	27.9	0.55	1.76	6.91	5.46	4.75	4.60	5.59	4.71
% 4/05-7	2005	3/7	1500	42.2	68.5	5.43	6.7	35.0	94.0	37.7	35.0	–	1.03	4.13	5.33	5.46	3.74	5.74	4.28
% 4/05-8	2005	3/21	1500	86.5	75.8	5.02	4.8	59.6	65.9	30.6	24.2	0.49	0.76	4.18	7.08	5.15	3.67	5.37	4.46
% 8/05-1	2005	4/8	1500	46.3	72.2	5.20	6.4	64.8	84.8	37.5	17.2	0.50	0.55	2.46	6.03	4.65	3.99	5.38	4.40
% 11/05-2	2005	8/24	1500	20.1	60.4	6.14	7.1	45.3	59.8	34.3	29.3	0.58	1.40	5.53	6.06	5.42	3.98	5.68	4.74
% 11/05-4-2	2005	9/22	1500	30.6	60.5	7.30	6.8	48.8	92.9	39.7	27.2	0.78	1.91	7.78	5.77	5.41	3.60	–	4.19
% 8/06-2	2006	5/16	1500	38.9	59.8	8.00	5.9	55.0	81.9	21.7	32.5	0.44	1.12	5.51	5.82	5.17	3.88	5.31	–
% 8/06-3	2006	5/31	1500	25.9	59.1	6.56	5.8	60.9	64.2	27.0	18.1	–	1.80	8.68	6.26	5.20	4.01	5.39	3.98
% 8/06-5	2006	7/1	1500	32.2	60.5	7.21	7.1	28.2	51.9	55.5	33.7	0.57	1.03	6.16	5.33	5.23	4.11	5.44	4.78
% 8/06-6	2006	7/17	1500	34.3	63.1	8.41	6.9	76.1	35.8	14.7	22.0	0.78	1.00	5.92	5.93	5.12	–	5.2	4.81
% 8/06-7	2006	8/2	1500	21.1	59.4	6.92	8.2	105.4	45.5	29.5	16.7	–	1.25	6.17	4.62	5.32	3.53	5.26	4.71
% 8/06-8	2006	8/17	1500	26.9	65.1	6.02	6.6	57.4	38.4	25.2	26.6	0.58	2.09	6.34	5.37	5.21	3.95	5.31	4.57
% 12/06-1	2006	9/3	1500	13.1	55.7	6.25	8.6	62.1	37.5	37.7	34.4	0.79	1.66	6.81	6.19	5.31	3.78	5.46	4.36
% 12/06-2	2006	9/18	1500	21.4	62.0	3.51	6.9	37.8	64.0	20.7	45.3	–	1.48	7.15	5.71	5.44	3.42	5.75	4.37
% 12/06-3	2006	10/3	1500	23.9	60.3	6.51	6.2	54.6	50.0	20.4	36.6	0.63	1.71	7.48	5.48	5.43	4.18	5.69	3.90
% 12/06-4	2006	10/19	1500	28.7	63.5	5.96	6.3	15.6	82.7	34.9	42.7	0.59	1.46	6.65	5.28	5.55	3.68	5.83	4.60
% 12/06-6	2006	11/18	1500	25.2	56.2	4.98	6.7	50.1	45.9	19.2	31.0	–	1.31	6.82	5.36	5.62	4.49	5.73	3.94
% 8/07-4	2007	5/19	1500	29.7	61.5	4.91	5.6	57.8	44.5	14.7	28.9	0.47	1.17	6.19	5.72	4.99	4.04	5.67	4.53
% 4/07-2	2006	1/4	1500	37.7	59.5	7.47	6.9	52.8	71.7	39.3	43.6	0.52	1.28	6.88	4.57	5.21	3.77	5.88	4.17
% 4/07-3	2007	1/20	1500	35.6	65.7	7.17	6.7	47.7	74.3	34.9	37.1	0.77	1.09	6.34	5.57	5.49	3.95	5.55	4.47
% 4/05-4	2005	1/25	3200	22.4	56.2	6.80	5.4	27.8	48.9	8.5	31.4	–	1.75	8.12	5.44	5.21	4.20	5.63	4.34
% 4/05-5	2005	2/8	3200	32.4	57.5	8.05	6.3	17.2	43.1	7.3	37.2	0.54	1.38	8.36	5.85	5.32	4.23	5.65	4.54
% 4/05-6	2005	2/22	3200	58.3	67.4	7.48	5.5	50.7	36.2	6.1	40.6	–	1.26	7.01	5.69	5.48	3.85	5.43	4.60

Appendix 1 (continued)

Sample ID	Year	Mid sampling date	Depth (m)	Flux (mg/m ² /d)	CaCO ₃ (%)	Si (%)	OC (%)	TCHO (mg/g)	Protein (mg/g)	URA (mg/g)	HS (mg/g)	HQ (mg/g)	Mn (mg/g)	Fe (mg/g)	logK _d (Th)	logK _d (Pa)	logK _d (Pb)	logK _d (Po)	logK _d (Be)
% 4/05-7	2005	3/7	3200	45.4	59.4	9.31	5.7	35.3	33.2	4.0	40.4	–	1.40	7.23	5.49	5.26	3.96	5.49	4.51
% 4/05-8	2005	3/21	3200	55.7	65.7	6.84	5.3	46.2	48.3	4.3	34.3	–	0.93	7.04	5.74	5.11	3.81	5.58	4.42
% 8/05-1	2005	4/8	3200	39.2	70.0	5.78	5.1	49.5	59.7	7.2	22.6	–	0.49	3.30	5.20	5.13	3.99	5.41	4.32
% 11/05-2	2005	8/24	3200	24.9	55.6	6.76	4.7	12.3	42.6	6.7	30.4	–	1.41	7.59	6.21	5.42	4.41	5.68	4.18
% 11/05-4	2005	9/22	3200	30.1	57.8	8.21	4.3	28.5	48.9	7.2	27.3	–	1.35	8.83	5.72	5.27	4.03	5.7	4.32
% 4/06-5	2006	1/26	3200	60.3	61.3	5.33	5.2	33.9	57.8	5.8	28.3	–	1.26	7.77	5.88	5.30	4.32	5.55	4.17
% 4/06-7	2006	2/27	3200	60.7	61.5	7.23	5.7	38.9	49.1	5.1	30.8	–	1.31	8.01	5.29	5.33	3.88	5.83	4.46
% 4/06-10	2006	4/13	3200	67.8	65.9	7.07	4.1	46.4	45.5	6.3	27.5	–	0.97	6.10	5.63	5.01	3.68	5.61	–
% 8/06-2	2006	5/16	3200	39.5	61.6	7.06	4.5	29.3	37.6	9.6	19.4	0.27	1.17	7.74	4.89	5.32	4.43	5.42	4.58
% 8/06-3	2006	5/31	3200	34.4	58.6	5.20	4.7	41.7	30.2	9.4	16.3	–	1.29	7.66	5.08	5.13	4.16	5.38	4.28
% 8/06-5	2006	7/1	3200	41.7	62.0	5.23	4.7	24.2	31.5	8.4	25.4	–	1.51	8.37	5.17	4.84	4.10	5.42	4.70
% 8/06-6	2006	7/17	3200	34.4	60.2	7.67	4.3	41.6	29.1	6.2	20.4	–	1.20	7.44	5.44	5.27	4.07	5.64	4.67
% 8/06-7	2006	8/2	3200	32.4	64.2	5.85	4.8	19.9	60.2	6.7	36.2	0.49	1.18	7.13	5.49	5.07	3.52	5.76	4.34
% 8/06-8	2006	8/17	3200	24.7	61.5	7.38	4.8	25.3	39.1	6.4	27.5	–	1.68	7.94	5.29	4.94	4.45	5.72	4.62
% 12/06-1	2006	9/2	3200	8.2	57.5	7.87	5.9	–	41.1	4.8	–	–	–	5.91	5.49	4.05	5.73	4.43	–
% 12/06-2	2006	9/17	3200	13.4	54.5	6.07	5.1	20.4	41.7	5.9	30.8	–	1.57	7.50	5.37	5.14	4.17	5.87	3.86
% 12/06-3	2006	10/2	3200	30.8	63.6	6.59	4.7	28.9	38.3	4.6	26.1	–	1.63	7.72	5.27	4.98	4.20	5.85	4.51
% 12/06-4	2006	10/18	3200	19.2	62.4	5.95	5.2	11.1	41.9	9.0	32.3	–	1.35	7.69	5.78	5.25	3.96	5.84	4.42
% 12/06-6	2006	11/17	3200	22.9	61.6	6.87	4.8	31.3	51.3	5.7	27.8	–	1.44	8.23	5.47	5.38	4.29	5.84	4.60
% 4/07-2	2006	1/4	3200	31.4	62.0	7.93	5.8	64.2	47.8	5.5	20.7	0.59	1.33	7.95	5.88	5.67	4.35	5.72	4.58
% 4/07-3	2007	1/20	3200	46.3	62.3	7.99	4.9	38.0	66.7	5.4	26.0	–	1.51	7.87	5.40	5.34	3.67	5.84	4.55
% 8/07-4	2007	5/19	3200	32.2	57.8	7.12	4.2	19.3	59.2	8.2	23.6	–	1.28	7.55	5.69	5.28	3.94	5.84	4.62

Appendix 2. Elemental composition and their possible % shale contribution in OFP sediment trap particles

Element	Total (ppm)				Contribution from shale			Net (= total – shale contribution)			% shale contribution		
	Shale	500 m	1500 m	3200 m	500 m	1500 m	3200 m	500 m	1500 m	3200 m	500 m	1500 m	3200 m
OC	12,000	171,000	74,000	54,000	675	1514	2090	170,325	72,486	51,910	0.39	2.05	3.87
N	1000	24,000	10,000	6200	56	126	174	23,944	9874	6026	0.23	1.26	2.81
Mg	15,000	4474	5641	6128	844	1892	2613	3630	3749	3515	18.86	33.54	42.64
Al	87,000	4893	10,975	15,154	4893	10,975	15,154	0	0	0	100.00	100.00	100.00
Si	275,000	50,390	99,471	126,904	15,466	34,691	47,901	34,924	64,780	79,003	30.69	34.88	37.75
P	700	2249	911	700	39	88	122	2210	823	578	1.75	9.69	17.42
Ca	16,000	267,341	260,918	253,605	900	2018	2787	266,441	258,900	250,818	0.34	0.77	1.10
Sc	13	0.70	1.50	2.00	0.73	1.64	2.26	–0.03	–0.14	–0.26	104.45	109.33	113.22
Ti	4600	200	406	599	259	580	801	–59	–174	–202	129	143	134
V	130	7.80	21.20	30.20	7.31	16.40	22.64	0.49	4.80	7.56	93.74	77.36	74.98
Mn	850	191	927	1119	48	107	148	143	820	971	25	12	13
Fe	47,200	2943	6651	9367	2655	5954	8221	288	697	1146	90	90	88
Co	19	3.90	11.50	13.20	1.1	2.4	3.3	2.8	9.1	9.9	27.4	20.8	25.1
Ni	50	33	39	42	2.8	6.3	8.7	30.2	32.4	33.6	8.5	16.3	20.6
Cu	45	49	58	73	2.5	5.7	7.8	46.5	52.3	65.2	5.2	9.8	10.7
Zn	95	114	107	84	5.3	12.0	16.5	108.7	95.0	67.5	4.7	11.2	19.7
Sr	170	1743	1831	1759	9.6	21.4	29.6	1733	1810	1729	0.5	1.2	1.7
Cd	0.3	2.7	1	0.51	0.02	0.04	0.05	2.68	0.96	0.46	0.62	3.78	10.25
Ba	580	401	842	818	33	73	101	368	769	717	8	9	12
Pb	20	42	56	75	1.1	2.5	3.5	40.9	53.5	71.5	2.7	4.5	4.6

Bold numbers indicate the element measured in this study. Bold and underline emphases the reference element for the calculation of this study.

References

- Ahrland, S., Liljenzin, J.O., Rydberg, J., 1973. Solution chemistry. In: Bailar, J.C., Trotman-Dickenson, A.F. (Eds.), *Comprehensive Inorganic Chemistry*. Oxford Pergamon Exclusive Distributors in Western Hemisphere, Compendium Publishers, Oxford.
- Albrecht-Gary, A.M., Crumbliss, A.L., 1998. Coordination chemistry of siderophores: thermodynamics and kinetics of iron chelation and release. *Met. Ions Biol. Syst.* 35, 239–327.
- Alvarado Quiroz, N.G., Hung, C.-C., Santschi, P.H., 2006. Binding of thorium(IV) to carboxylate, phosphate and sulfate functional groups from marine copolymeric substances (EPS). *Mar. Chem.* 100 (3–4), 337–353.
- Arnou, L.E., 1937. Colorimetric determination of the components of 3,4-dihydroxyphenylalanine-tyrosine mixtures. *J. Biol. Chem.* 118 (2), 531–537.
- Baskaran, M., Santschi, P.H., 1993. The role of particles and colloids in the transport of radionuclides in coastal environments of Texas. *Mar. Chem.* 43 (1–4), 95–114.
- Baskaran, M., Santschi, P.H., 2002. Particulate and dissolved ²¹⁰Pb activities in the shelf and slope regions of the Gulf of Mexico waters. *Cont. Shelf Res.* 22 (10), 1493–1510.
- Baskaran, M., Swarzenski, P.W., 2007. Seasonal variations on the residence times and partitioning of short-lived radionuclides (²³⁴Th, ⁷Be and ²¹⁰Pb) and depositional fluxes of ⁷Be and ²¹⁰Pb in Tampa Bay, Florida. *Mar. Chem.* 104 (1–2), 27–42.
- Baskaran, M., Ravichandran, M., Bianchi, T.S., 1997. Cycling of ⁷Be and ²¹⁰Pb in a high DOC, shallow, turbid estuary of south-east Texas. *Estuar. Coast. Shelf Sci.* 45 (2), 165–176.
- Boye, M., van den Berg, C.M.G., de Jong, J.T.M., Leach, H., Croot, P., de Baar, H.J.W., 2001. Organic complexation of iron in the Southern Ocean. *Deep-Sea Res. I Oceanogr. Res. Pap.* 48 (6), 1477–1497.
- Broecker, W.S., Peng, T., 1982. *Tracers in the Sea*. 690.
- Brown, D.A., McKeith, D., Glass, W.K., 1979. Transition metal complexes of monohydroxamic acids. *Inorg. Chim. Acta* 35, 5–10.
- Chase, Z., Anderson, R.F., Fleisher, M.Q., Kubik, P.W., 2002. The influence of particle composition and particle flux on scavenging of Th, Pa and Be in the ocean. *Earth Planet. Sci. Lett.* 204 (1–2), 215–229.
- Choppin, G.R., 1983. Comparison of the solution chemistry of the actinides and lanthanides. *J. Less-Common Met.* 93 (2), 323–330.
- Chuang, C.-Y., Ho, Y.-F., Santschi, P.H., 2013a. Is biogenic silica responsible for scavenging of radionuclides, ²³⁴Th, ²³³Pa, ²¹⁰Pb, ²¹⁰Po, ⁷Be, in the ocean? A case study with *Phaeodactylum Tricornutum*. ASLO 2013 Aquatic Sciences Meeting, New Orleans, Louisiana, USA.
- Chuang, C.-Y., Santschi, P.H., Jiang, Y., Ho, Y.-F., Quigg, A., Guo, L.D., Ayrarov, M., Schumann, D., 2013b. Role of diatoms in the scavenging of particle reactive radionuclides, thorium, protactinium, lead, polonium and beryllium, in the ocean: a case study with *Phaeodactylum tricornutum*. *Limnol. Oceanogr.* (in Revision).

- Ciffroy, P., Reys, J.-L., Siclet, F., 2003. Determination of the residence time of suspended particles in the turbidity maximum of the Loire estuary by ^7Be analysis. *Estuar. Coast. Shelf Sci.* 57 (4), 553–568.
- Conte, M.H., Ralph, N., Ross, E.H., 2001. Seasonal and interannual variability in deep ocean particle fluxes at the Oceanic Flux Program (OFP)/Bermuda Atlantic Time Series (BATS) site in the western Sargasso Sea near Bermuda. *Deep-Sea Res. II Top. Stud. Oceanogr.* 48 (8–9), 1471–1505.
- Csáky, T.Z., 1948. An estimation of bound hydroxylamine in biological materials. *Acta Chem. Scand.* 2, 450–454.
- Dhungana, S., Ratledge, C., Crumbliss, A.L., 2004. Iron chelation properties of an extracellular siderophore exochelin MS. *Inorg. Chem.* 43 (20), 6274–6283.
- Doucet, F.J., Schneider, C., Bones, S.J., Kretschmer, A., Moss, I., Tekely, P., Exley, C., 2001. The formation of hydroxylaluminosilicates of geochemical and biological significance. *Geochim. Cosmochim. Acta* 65 (15), 2461–2467.
- Duckworth, O.W., Bargar, J.R., Sposito, G., 2008. Sorption of ferric iron from ferrioxamine B to synthetic and biogenic layer type manganese oxides. *Geochim. Cosmochim. Acta* 72 (14), 3371–3380.
- Filissetti-Cozzi, T.M.C.C., Carpita, N.C., 1991. Measurement of uronic acids without interference from neutral sugars. *Anal. Biochem.* 197 (1), 157–162.
- Geibert, W., Usbeck, R., 2004. Adsorption of thorium and protactinium onto different particle types: experimental findings. *Geochim. Cosmochim. Acta* 68 (7), 1489–1501.
- Geszvain, K., Yamaguchi, A., Maybee, J., Tebo, B., 2011. Mn(II) oxidation in *Pseudomonas putida* GB-1 is influenced by flagella synthesis and surface substrate. *Arch. Microbiol.* 193 (8), 605–614.
- Geszvain, K., McCarthy, J.K., Tebo, B.M., 2013. Elimination of manganese(II, III) oxidation in *Pseudomonas putida* GB-1 by a double knockout of two putative multicopper oxidase genes. *Appl. Environ. Microbiol.* 79 (1), 357–366.
- Gledhill, M., Van Den Berg, C.M.G., 1994. Determination of complexation of iron(III) with natural organic complexing ligands in seawater using cathodic stripping voltammetry. *Mar. Chem.* 47 (1), 41–54.
- Guo, L.D., Santschi, P.H., Baskaran, M., Zindler, A., 1995. Distribution of dissolved and particulate ^{230}Th and ^{232}Th in seawater from the Gulf of Mexico and off Cape Hatteras as measured by SIMS. *Earth Planet. Sci. Lett.* 133 (1–2), 117–128.
- Guo, L.D., Santschi, P.H., Baskaran, M., 1997. Interactions of thorium isotopes with colloidal organic matter in oceanic environments. *Colloids Surf. A* 120 (1–3), 255–271.
- Guo, L.D., Chen, M., Gueguen, C., 2002a. Control of Pa/Th ratio by particulate chemical composition. *Geophys. Res. Lett.* 29, 1960.
- Guo, L.D., Hung, C.C., Santschi, P.H., Walsh, I.D., 2002b. ^{234}Th scavenging and its relationship to acid polysaccharide abundance in the Gulf of Mexico. *Mar. Chem.* 78 (2–3), 103–119.
- Harrington, J.M., Parker, D.L., Bargar, J.R., Jarzecki, A.A., Tebo, B.M., Sposito, G., Duckworth, O.W., 2012. Structural dependence of Mn complexation by siderophores: donor group dependence on complex stability and reactivity. *Geochim. Cosmochim. Acta* 88, 106–119.
- Hauptkorn, S., Pavel, J., Seltner, H., 2001. Determination of silicon in biological samples by ICP-OES after non-oxidative decomposition under alkaline conditions. *Fresenius J. Anal. Chem.* 370 (2), 246–250.
- Hirose, K., 1995. The relationship between particulate uranium and thorium-complexing capacity of oceanic particulate matter. *Sci. Total Environ.* 173 (1–6), 195–201.
- Hirose, K., Tanoue, E., 2001. Strong ligands for thorium complexation in marine bacteria. *Mar. Environ. Res.* 51 (2), 95–112.
- Honeyman, B.D., Santschi, P.H., 1989. A Brownian-pumping model for oceanic trace-metal scavenging – evidence from Th-isotopes. *J. Mar. Res.* 47 (4), 951–992.
- Huang, S., Conte, M.H., 2009. Source/process apportionment of major and trace elements in sinking particles in the Sargasso sea. *Geochim. Cosmochim. Acta* 73 (1), 65–90.
- Huang, S., Sholkovitz, E.R., Conte, M.H., 2007. Application of high-temperature fusion for analysis of major and trace elements in marine sediment trap samples. *Limnol. Oceanogr. Methods* 5, 13–22.
- Hung, C.C., Santschi, P.H., 2001. Spectrophotometric determination of total uronic acids in seawater using cation-exchange separation and pre-concentration by lyophilization. *Anal. Chim. Acta.* 427 (1), 111–117.
- Hussain, N., Ferdelman, T.G., Church, T.M., Luther III, G., 1995. Bio-volatilization of polonium: results from laboratory analyses. *Aquat. Geochem.* 1 (2), 175–188.
- Jiao, N., Herndl, G.J., Hansell, D.A., Benner, R., Kattner, G., Wilhelm, S.W., Kirchman, D.L., Weinbauer, M.G., Luo, T., Chen, F., Azam, F., 2010. Microbial production of recalcitrant dissolved organic matter: long-term carbon storage in the global ocean. *Nat. Rev. Microbiol.* 8 (8), 593–599.
- Kalmykov, S.N., Schäfer, T., Claret, F., Perminova, I.V., Petrova, A.B., Shcherbina, N.S., Teterin, Y.A., 2008. Sorption of neptunium onto goethite in the presence of humic acids with different hydroquinone group content. *Radiochim. Acta* 96 (9–11), 685–690.
- Keith-Roach, M.J., Buratti, M.V., Worsfold, P.J., 2005. Thorium complexation by hydroxamate siderophores in perturbed multicomponent systems using flow injection electrospray ionization mass spectrometry. *Anal. Chem.* 77 (22), 7335–7341.
- Kim, G., Hussain, N., Church, T.M., 2003a. Tracing the advection of organic carbon into the subsurface Sargasso Sea using a $^{228}\text{Ra}/^{226}\text{Ra}$ tracer. *Geophys. Res. Lett.* 30 (16), 1874.
- Kim, M.A., Panak, P.J., Yun, J.J., Kim, J.J., Klenze, R., Kohler, K., 2003b. Interaction of actinides with aluminosilicate colloids in statu nascendi Part I: generation and characterization of actinide(III)-pseudocolloids. *Colloids Surf. A* 216 (1–3), 97–108.
- Kondo, Y., Takeda, S., Furuya, K., 2012. Distinct trends in dissolved Fe speciation between shallow and deep waters in the Pacific Ocean. *Mar. Chem.* 134–135, 18–28.
- Kretschmer, S., Geibert, W., van der Loeff, M.M.R., Schnabel, C., Xu, S., Mollenhauer, G., 2011. Fractionation of ^{230}Th , ^{231}Pa , and ^{10}Be induced by particle size and composition within an opal-rich sediment of the Atlantic Southern Ocean. *Geochim. Cosmochim. Acta* 75 (22), 6971–6987.
- Kröger, N., Lorenz, S., Brunner, E., Sumper, M., 2002. Self-assembly of highly phosphorylated silaffins and their function in biosilica morphogenesis. *Science* 298 (5593), 584–586.
- Kurzak, B., Kozłowski, H., Farkas, E., 1992. ChemInform abstract: hydroxamic and aminohydroxamic acids and their complexes with metal ions. *ChemInform* 23 (40).
- Lam, P.J., Bishop, J.K., Waychunas, G.A., Sutton, S.R., Newville, M., 2002. Characterization of Fe in marine particulates via micro-XAS: possibilities and limitations. APS Activity Report 2001. Argonne National Lab Laboratory, Argonne, IL (ANL-02/06).
- Lam, P.J., Ohnemus, D.C., Marcus, M.A., 2012. The speciation of marine particulate iron adjacent to active and passive continental margins. *Geochim. Cosmochim. Acta* 80, 108–124.
- Lee, C., Wakeham, S., Amosti, C., 2004. Particulate organic matter in the sea: the composition conundrum. *Ambio* 33 (8), 565–575.
- Li, Y.-H., 1991. Distribution patterns of the elements in the ocean: a synthesis. *Geochim. Cosmochim. Acta* 55 (11), 3223–3240.
- Li, Y.-H., 2000. A Compendium of Geochemistry: From Solar Nebula to the Human Brain. Princeton University Press.
- Li, Y.-H., 2005. Controversy over the relationship between major components of sediment-trap materials and the bulk distribution coefficients of ^{230}Th , ^{231}Pa , and ^{10}Be . *Earth Planet. Sci. Lett.* 233 (1–2), 1–7.
- Li, Y.-H., Burkhardt, L., Buchholtz, M., Ohara, P., Santschi, P.H., 1984. Partition of radio-tracers between suspended particles and seawater. *Geochim. Cosmochim. Acta* 48 (10), 2011–2019.
- Madison, A.S., Tebo, B.M., Luther III, G.W., 2011. Simultaneous determination of soluble manganese(III), manganese(II) and total manganese in natural (pore)waters. *Talanta* 84 (2), 374–381.
- Marquardt, C.M., Panak, P.J., Apostolidis, C., Morgenstern, A., Walther, C., Klenze, R., Fanghänel, T., 2004. Fluorescence spectroscopy on protactinium(IV) in aqueous solution. *Radiochim. Acta* 92 (7–2004), 445–447.
- Masque, P., Sanchez-Cabeza, J.A., Bruach, J.M., Palacios, E., Canals, M., 2002. Balance and residence times of ^{210}Pb and ^{210}Po in surface waters of the northwestern Mediterranean Sea. *Cont. Shelf Res.* 22 (15), 2127–2146.
- Mawji, E., Gledhill, M., Milton, J.A., Tarran, G.A., Ussher, S., Thompson, A., Wolff, G.A., Worsfold, P.J., Achterberg, E.P., 2008. Hydroxamate siderophores: occurrence and importance in the Atlantic Ocean. *Environ. Sci. Technol.* 42 (23), 8675–8680.
- Menzel, D.W., Ryther, J.H., 1959. The annual cycle of primary production in the Sargasso Sea off Bermuda. *Deep-Sea Res.* 6, 351–367 (1953).
- Moran, S.B., Shen, C.C., Edmonds, H.N., Weinstein, S.E., Smith, J.N., Edwards, R.L., 2002. Dissolved and particulate ^{231}Pa and ^{230}Th in the Atlantic Ocean: constraints on intermediate/deep water age, boundary scavenging, and $^{231}\text{Pa}/^{230}\text{Th}$ fractionation. *Earth Planet. Sci. Lett.* 203 (3–4), 999–1014.
- National Research Council, C.o.W.Q.C., 1972. Suspended particulate materials, water quality criteria, 1972: a report of the Committee on Water Quality Criteria, Environmental Studies Board, National Academy of Sciences, National Academy of Engineering, Washington, D.C., 1972. Environmental Protection Agency: for sale by the Supt. of Docs., U.S. Govt. Print. Off.
- Neilands, J.B., 1995. Siderophores – structure and function of microbial iron transport compounds. *J. Biol. Chem.* 270 (45), 26723–26726.
- Neu, M.P., Matonic, J.H., Ruggiero, C.E., Scott, B.L., 2000. Structural characterization of a plutonium(IV) siderophore complex: single-crystal structure of Pu-desferrioxamine E. *Angew. Chem. Int. Ed.* 39 (8), 1442–1444.
- Nyffeler, U.P., Li, Y.-H., Santschi, P.H., 1984. A kinetic approach to describe trace-element distribution between particles and solution in natural aquatic systems. *Geochim. Cosmochim. Acta* 48 (7), 1513–1522.
- Panak, P.J., Kim, M.A., Yun, J.J., Kim, J.J., 2003. Interaction of actinides with aluminosilicate colloids in statu nascendi. Part II: spectroscopic speciation of colloid-borne actinides(III). *Colloids Surf. A* 227 (1–3), 93–103.
- Poulsen, N., Sumper, M., Kroger, N., 2003. Biosilica formation in diatoms: characterization of native silaffin-2 and its role in silica morphogenesis. *Proc. Natl. Acad. Sci. U. S. A.* 100 (21), 12075–12080.
- Quigley, M.S., Santschi, P.H., Hung, C.C., Guo, L.D., Honeyman, B.D., 2002. Importance of acid polysaccharides for ^{234}Th complexation to marine organic matter. *Limnol. Oceanogr.* 47 (2), 367–377.
- Reid, R.T., Live, D.H., Faulkner, D.J., Butler, A., 1993. A siderophore from a marine bacterium with an exceptional ferric ion affinity constant. *Nature* 366 (6454), 455–458.
- Roberts, K.A., Xu, C., Hung, C.C., Conte, M.H., Santschi, P.H., 2009. Scavenging and fractionation of thorium vs. protactinium in the ocean, as determined from particle-water partitioning experiments with sediment trap material from the Gulf of Mexico and Sargasso Sea. *Earth Planet. Sci. Lett.* 286 (1–2), 131–138.
- Rue, E.L., Bruland, K.W., 1995. Complexation of iron(III) by natural organic-ligands in the Central North Pacific as determined by a new competitive ligand equilibration adsorptive cathodic stripping voltammetric method. *Mar. Chem.* 50 (1–4), 117–138.
- Rutgers van der Loeff, M.M., Berger, G.W., 1993. Scavenging of ^{230}Th and ^{231}Pa near the antarctic polar front in the South Atlantic. *Deep-Sea Res. I Oceanogr. Res. Pap.* 40 (2), 339–357.
- Santschi, P.H., Guo, L.D., Baskaran, M., Trumbore, S., Southon, J., Bianchi, T.S., Honeyman, B., Cifuentes, L., 1995. Isotopic evidence for the contemporary origin of high-molecular weight organic matter in oceanic environments. *Geochim. Cosmochim. Acta* 59 (3), 625–631.
- Santschi, P.H., Roberts, K.A., Guo, L.D., 2002. Organic nature of colloidal actinides transported in surface water environments. *Environ. Sci. Technol.* 36 (17), 3711–3719.
- Santschi, P.H., Murray, J.W., Baskaran, M., Benitez-Nelson, C.R., Guo, L.D., Hung, C.C., Lamborg, C., Moran, S.B., Passow, U., Roy-Barman, M., 2006. Thorium speciation in seawater. *Mar. Chem.* 100 (3–4), 250–268.
- Schindler, P.W., 1975. Removal of trace metals from the oceans: a zero order model. In: C.z.I. Mora and J.a.z.i.u.B. institut (Ed.), *Thalassia Jugoslavica*. Center for Marine Research, pp. 101–111.

- Schindler, P.W., Stumm, W., 1987. The surface chemistry of oxides, hydroxides and oxide minerals. In: Stumm, W. (Ed.), *Aquatic Surface Chemistry: Chemical Processes at the Particle–Water Interface*. John Wiley & Sons Inc., pp. 83–110.
- Schindler, P.W., Fürst, B., Dick, R., Wolf, P.U., 1976. Ligand properties of surface silanol groups. I. Surface complex formation with Fe^{3+} , Cu^{2+} , Cd^{2+} , and Pb^{2+} . *J. Colloid Interface Sci.* 55 (2), 469–475.
- Scholten, J.C., Fietzke, J., Mangini, A., Stoffers, P., Rixen, T., Gaye-Haake, B., Blanz, T., Ramaswamy, V., Sirocko, F., Schulz, H., Ittekkot, V., 2005. Radionuclide fluxes in the Arabian Sea: the role of particle composition. *Earth Planet. Sci. Lett.* 230 (3–4), 319–337.
- Schumann, D., Ayranov, M., Stowasser, T., Gialanella, L., Leva, A.D., Romano, M., Schuermann, D., 2013. Radiochemical separation of ^7Be from the cooling water of the neutron spallation source SINQ at PSI. *Radiochim. Acta* 101, 509–514.
- Sirajuddin, Bhangar, M.L., Niaz, A., Shah, A., Rauf, A., 2007. Ultra-trace level determination of hydroquinone in waste photographic solutions by UV–vis spectrophotometry. *Talanta* 72 (2), 546–553.
- Spiro, T.G., Bargar, J.R., Sposito, G., Tebo, B.M., 2009. Bacteriogenic manganese oxides. *Acc. Chem. Res.* 43 (1), 2–9.
- Strickland, J.D.H., Parsons, T.R., 1972. *A practical handbook of seawater analysis*. Bulletin, 167. Fisheries Research Board of Canada, Ottawa.
- Stumm, W., Morgan, J.J., 1996. *Chemical equilibria and rates in natural waters, aquatic chemistry*. John Wiley & Sons, Inc., New York 1022.
- Tateda, Y., Carvalho, F.P., Fowler, S.W., Miquel, J.-C., 2003. Fractionation of ^{210}Po and ^{210}Pb in coastal waters of the NW Mediterranean continental margin. *Cont. Shelf Res.* 23 (3–4), 295–316.
- Toner, B.M., Marcus, M.A., Edwards, K.J., Rouxel, O., German, C.R., 2012. Measuring the form of iron in hydrothermal plume particles. *Oceanography* 25 (1), 209–212.
- Wieneke, R., Bernecker, A., Riedel, R., Sumper, M., Steinem, C., Geyer, A., 2011. Silica precipitation with synthetic silaffin peptides. *Org. Biomol. Chem.* 9 (15), 5482–5486.
- Winkelmann, G., 2002. Microbial siderophore-mediated transport. *Biochem. Soc. Trans.* 30, 691–696.
- Woźniak, S.B., Stramski, D., Stramska, M., Reynolds, R.A., Wright, V.M., Miksic, E.Y., Cichocka, M., Cieplak, A.M., 2010. Optical variability of seawater in relation to particle concentration, composition, and size distribution in the nearshore marine environment at Imperial Beach, California. *J. Geophys. Res. Oceans* 115 (C8), C08027.
- Xu, C., Santschi, P.H., Zhong, J.Y., Hatcher, P.G., Francis, A.J., Dodge, C.J., Roberts, K.A., Hung, C.C., Honeyman, B.D., 2008. Colloidal cutin-like substances cross-linked to siderophore decomposition products mobilizing plutonium from contaminated soils. *Environ. Sci. Technol.* 42 (22), 8211–8217.
- Xu, C., Santschi, P.H., Schwehr, K.A., Hung, C.C., 2009. Optimized isolation procedure for obtaining strongly actinide binding exopolymeric substances (EPS) from two bacteria (*Sagittula stellata* and *Pseudomonas fluorescens* Biovar II). *Bioresour. Technol.* 100 (23), 6010–6021.
- Xu, C., Zhang, S.J., Chuang, C.Y., Miller, E.J., Schwehr, K.A., Santschi, P.H., 2011. Chemical composition and relative hydrophobicity of microbial exopolymeric substances (EPS) isolated by anion exchange chromatography and their actinide-binding affinities. *Mar. Chem.* 126 (1–4), 27–36.
- Xu, C., Chen, H., Sugiyama, Y., Zhang, S., Li, H.-P., Ho, Y.-F., Chuang, C.-Y., Schwehr, K.A., Kaplan, D.L., Yeager, C., Roberts, K.A., Hatcher, P.G., Santschi, P.H., 2013. Novel molecular-level evidence of iodine binding to natural organic matter from Fourier transform ion cyclotron resonance mass spectrometry. *Sci. Total Environ.* 449, 244–252.
- Yang, W., Guo, L., Chuang, C.-Y., Schumann, D., Ayranov, M., Santschi, P.H., 2013. Adsorption characteristics of ^{210}Pb , ^{210}Po and ^7Be onto micro-particle surfaces and the effects of macromolecular organic compounds. *Geochim. Cosmochim. Acta* 107, 47–64.
- Zeh, P., Kim, J.L., Marquardt, C.M., Artinger, R., 1999. The reduction of Np(V) in groundwater rich in humic substances. *Radiochim. Acta* 87 (1–2), 23–28.
- Zuo, Z., Eisma, D., 1993. ^{210}Pb and ^{210}Po distributions and disequilibrium in the coastal and shelf waters of the southern North Sea. *Cont. Shelf Res.* 13 (8–9), 999–1022.